Mapping and analysis of structural lineaments using SRTM radar data and Landsat 8-OLI images in Telouet-Tighza area, Marrakech High Atlas - Morocco.

maryam errami (maryamerrami@gmail.com)
Cadi Ayyad University: Universite Cadi Ayyad https://orcid.org/0000-0002-0452-6996
Ahmed ALGOUTI
Cadi Ayyad University: Universite Cadi Ayyad
Abdellah ALGOUTI
Cadi Ayyad University: Universite Cadi Ayyad
Abdelouahed FARAH
Cadi Ayyad University: Universite Cadi Ayyad

Research Article

Keywords: Marrakech High Atlas, Telouet-Tighza, Remote Sensing, Landsat-8 OLI, SRTM data, Automatic Lineament Extraction

Posted Date: February 25th, 2022

DOI: https://doi.org/10.21203/rs.3.rs-1153424/v1

Abstract

Certainly, remote sensing data more specifically Landsat 8 Operational Land Imager and SRTM images can be used as a powerful tool for lineament mapping. Lineament extraction method and statistical studies are attractive an alternative analysis techniques which resolve lineament mapping problems in the region and allow exceeding the usual classical method. The present study deals with the estimation of the potential of both Landsat 8 Operational Land Imager sensor images and SRTM Digital Elevation Model data for automatic lineament extraction in the south side of Marrakech High Atlas (Telouet-Tighza area). After image corrections, enhancement methods such as principal component analysis (PCA), Band Composite and Directional Filter were adopted in order to create new images with high visibility of linear structures. A Principal Component Analysis (PCA) has been realized on the Landsat 8- OLI bands in order to reduce the redundancy information in highly correlated bands. Validating the use of the new Landsat band composite image relied on calculating statistical optimum index factor (OIF), Correlation Index and matching interpreted linear structures to previously published geologic maps. Therefore, the SRTM Digital Elevation Model is used in this study to generate shaded relief images as well as three-dimensional representation of the terrain and slope. Shaded relief images allowed to highlight linear features related to geomorphological data which are not identified in optical images. Multi-source data, such as Band Ratio image, geological map and fieldworks were used to verify and eliminate meaningless and non- geological lineaments extracted by applying line model tool of Geomatica software.

The results indicate that automatic method was applied successfully for lineament mapping in the Telouet-Tighza area and showing improvement over previous techniques in detailing the main tectonic faults. Slope and lithological factor were recognized to understand their relation with spatial distribution of lineaments over the study area. Structural lineaments generated from PC1, selected Band composite images and shaded relief DEM data proved the coincidence of their direction, length, and density with the tectonic system of the study area. The resultant fracture network is oriented ENE-WSW and E-W with a predominance of the E-W direction. It showsgood correlation between the distribution and the orientation of the lineaments on updated lineament map in comparison with the localization and orientation of fault system pattern in the existing geological map. In addition, the new synthetic structural map shows more information and details compared with based geological map which reveals the performance of Landsat 8-oli bands and SRTM data in this kind of study.

1. Introduction

Lineaments are considered to be a mappable, linear or curvilinear, simple or composed, feature exposed at the Earth's surface, they may correspond to natural objects such as structural alignment (fractures, faults, shear zones and line weakness), and geomorphologic consequences (caused by contrast differences, tonal or relief(Adiri et al. 2017). In general, linear features are caused by subtle brightness differences and by contrast differences in the image which produces edges. On the earth, these edges are expression of change in composition of natural objects. Consequently, they can represent boundaries of different land cover units (joints of stratigraphic formations, dykes, straight stream and valley, vegetation type and height, alignments in vegetation or soil tonal changes), abrupt topographic changes, or artificial features (roads, bridges, and edges)(Jellouli et al. 2021).A large number of lineament mapping and studies of geological structures were applied successfully in several geosciences' applications, especially in tectonic architecture, precious metals and petroleum exploration, nuclear energy studiesand groundwater exploration. The importance of lineaments related to fractures is manifested by their localization often close to several mineralogical deposits, oil, geothermal, and water reservoirs (A. B. Pour and Hashim 2015; Shandini et al. 2020).Furthermore, study of lineaments provide an excellent base information that can be used to understand both the orientation of tectonic stress and fracture kinematics in order to reconstruct regional tectonic history(Mhamdi et al. 2017). Structural and kinematic study of fractures systems provide fundamental information about deformational processes, and furnish insights about the tectonic framework and plate movements of a region (Saadi et al. 2011) as well as the relationship between local structural features and ongoing deformation (Fekkak et al. 2018).

In early times, manual approach which is produced by tracking faults in the fieldwork was the main method used in lineament mapping. This method is difficult, very laborious, time-consuming, and very demanding in terms of human and material. Therefore, they are highly dependent on the quality and objectivity of the analysis.

However, during the last two decades, the availability of cheaply multispectral remote sensing data and its high spatial and spectral resolution allows exploiting a variety of sources and methods in the characterization of lineaments, particularly automatic approach. The use of remote sensing and automatic approach in lineament mapping become more requested due to their advantages and strong advances to overcome the difficulties and limitations associated with lineament field mapping, especially in mountainous regions and poorly accessible terrain. Then, remote sensing offers a variety of multispectral data covering a large area and will provide a good alternative to traditional fieldwork in this region where the identification of geological structures is impeded by limited accessibility due to relief. In addition, remote sensing data have been widely used in lineaments mapping at various scales (Adiri et al. 2017; Hamdani and Baali 2019) and have shown a great success. Spaceborne multispectral sensors, especially Landsat 8- OLI have been well employed for such applications (Al-Djazouli et al. 2019; Azman, Ab Talib, and Sokiman 2020).

This study aims to evaluate the performance of Landsat 8 Operational Land Imager (OLI) multispectral satelliteand the Shuttle Radar Topography Mission (SRTM) digital elevation model in automatic lineaments extraction task. Integration of both the Landsat 8 OLI satellite images and Shuttle Radar Topography Mission (SRTM) digital elevation model allows the identification and mapping of possible deep structural lineaments in the Telouet-Tighza area with their statistics (numbers and frequencies of the lineaments, their distribution, directions, and densities). We highlighted the improvement of image processing techniques such as color band composites, spectral band ratios, PCA and directional edge-detection filters to enhance the analysis and interpretation of the structural lineaments. Firstly, Satellite data are subjected to the necessary topological corrections like noise removal, dimensionality reduction, and lineament enhancement. Secondly, line module algorithm embedded in the automatic method is used to detect and extract the multi-scale edges on Landsat 8 OLI and SRTM images by chosen of appropriate parameters for this operation. Finally, it is required to evaluate the quality and adequacy of lineaments identified via remote sensing. The extracted geological lineaments are checked and validated by superimposed topographic and geological maps of study area in order to

demonstrate the relationship between the lineaments resulted from spectral images processing and fractures mapped on the ground. In this last step, both the slope data and lithological map will help to understand the possible relationships between tectonic and the main lineaments of the region.

A number of studies have demonstrated the applicability of the automatic extraction by using Line Module algorithm for lineament mapping (Epuh et al. 2020; Shandini et al. 2020; Azman, Ab Talib, and Sokiman 2020). In Some works, lineament extraction was tried to be executed from only Landsat 8 OLI data. In the Moroccan Central Middle Atlas (Hamdani and Baali 2019) have applied the automatic extraction approach to Landsat 8 OLI data in order to identify the fracture network linked with the karst system. In addition, this sensor has previously showed great potential for lineament mapping of Jbel Tijekht mining area in Eastern Anti Atlas(Saidi et al. 2020) and in others Moroccan studies (Es-Sabbar et al. 2020; Bentahar, Raji, and Mhamdi 2020), which is undoubtedly due to its higher spatial and spectral resolution.

Other studies in Morocco used multisource data as a valuable source of information to accomplish their task by combining the Landsat 8-Oli images with other multispectral sensors to extract the maximum spectral info as well as to control and validate the obtained results. (Jellouli et al. 2021) applied the automatic lineament extraction using Landsat 8 OLI and ASTER data coupled to radar satellite images to extract lineaments in Kerdous inlier, Moroccan Anti Atlas. In another study,(Adiri et al. 2017)compare between the potential of Landsat-8 OLI, ASTER and Sentinel 1 multispectral data in lineament mapping of Sidi Flah-Bouskour inlier via Line Module algorithm.

Furthermore, other authors have found it suitable to extract lineament automatically by using high resolution Shuttle Radar Topography Mission (SRTM) and Landsat 8 OLI images as input. This approach, which consists of combining Shuttle Radar Topography Mission (SRTM) data and multispectrale images, has already been used in lineament mapping of many regions over the world with very good results. The results of two recently studies that have been achieved in Egypt by (Shandini et al. 2020)and(Abdelkareem et al. 2021) confirm the ability of SRTM data as an additional input to aid the spectral separability and to achieve the lineament mapping purposes. Therefore, the automatic extraction method applied on both Landsat 8 OLI and SRTM satellite data showed that these data can be used as a powerful tool to explore structural features and to further improve lineament mapping in several worldwide regions (Jawahar Raj and Prabhakaran 2018)(Aretouyap et al. 2020). In Morocco, (Abdelouhed, Ahmed, Abdellah, Mohammed, et al. 2021)demonstrated the effectiveness of Landsat 8 OLI and SRTM data to enhance the morphostructural lineaments in Ikniouen area, Eastern Anti Atlas.

The Telouet- Tighza inlier is situated in the southern flank of Marrakech High Atlas Belt between latitude 31°13'7"N and 31°34'44" N, and between longitude 7°43'46" W and 6°42'53" W. it covers an area of 258.449 Hectares (2584, 49 km^2) and a perimeter of 209, 28 km (Fig. 1B and C).It lies in the transition between tree provinces (Fig 1A and B). The north-western part lies within the Haouz province (in Marrakech Safi province), whereas the north-eastern part is belonging to the rural commune Ghessat (in Beni Mellal-Khenifra province). The Southern part of targeted area lies within the rural commune of Telouet (in Draa-Tafilalet province) (Fig 1A and B). The Marrakech High Atlas of Morocco lies to the south of the Haouz plain and to the north of the poorly developed foreland basins that forms the Late Cretaceous-Cenozoic discontinuous Souss-Ouarzazate basin (Fekkak et al. 2018). This part of High Atlas is oriented ENE and displays the highest elevations, at the former boundary between the Tethysian and Atlantic domain(Leprêtre et al. 2018). As a part of the High Atlas orogen, the Marrakech High Atlas has occurred during three orogenic cycles and it is subdivided in tree domains from the north to the south. The northern subatlasic zone is characterized by Jurassic-Cretaceous plateaus which are incorporated to the inner belt and lay unconformably on the Paleozoic basement (Saddiqi, Baidder, and Michard 2011). However, The axial zone displays large exposures of Precambrian to Paleozoic basement in many areas beside the faulted Triassic basins oriented NE- to ENE- (Domènech et al. 2015). At last, the southern subatlasic zone is characterized by Cretaceous to Cenozoic deposits attributed to post and syn- rift inversion with large calcareous plateaus developed toward the eastern transition with Central High Atlas (Domènech et al. 2015). To the West these units are very irregularly carved in a multitude of small witness mounds (Moret, n.d.). This part shows similar stratigraphic deposits with northern subatlasic zone, but Mesocenozoic cover is less folded here than its counterpart in the northern flank (Saddiqi, Baidder, and Michard 2011)

2. Geological Setting

The study area is situated in southern flank of Marrakech High Atlas Belt, about 100 km southeast of the Marrakech city (Fig.1B). It is characterized by rugged topography with the maximum elevation contained in the Tichka summit(Fig. 1C). In the geological map, Telouet- Tighza inlier encompasses part of the Marrakech High Atlas chain and small part of the Central High Atlas orogen (Fig. 2). It is covered by continuous geological sequences and various rock types ranging in age from Proterozoic rocks to Neogen alluvium formation (Fig.2). In addition to the overlaying Quaternary sediments, two major lithological groups are found in the target area; the Precambrian and Paleozoic basement rocks and the Meso-cenozoic sedimentary cover with the bigger part formed by Mesozoic rocks. The eastern part comprises the oldest rocks exposed in this area. This Precambrian basement rocks (Fig. 2) are built up of rhyolits, andesites and ignimbrites which outcrops also in small blocs in the western part. Precambrian units are unconformably overlain by volcano-clastic series of Ouarzazate group dated to terminal Precambrian and deposited after the panafricain collisional climax (Domènech et al. 2015). Thesmall outcrops of Precambrian rocks exposed in the western part of the studied area constitutes the eastern part of the famous block called ‘Massif central’ that is prolonged to the west of the study area (Moret, n.d.). These rocks cover approximately 137 km2 and are structured and metamorphosed during the Panafricain orogeny and possibly reworked by the Variscan and the Atlasic events (Michard, Ibouh, and Charrière 2011). The Paleozoic basement which outcrops in several exposures along Telouet-Tighza inlier is dominated by Cambro-Ordovician sedimentary formations (Fig.2). It includes middle Cambrian rocks called ‘Série lie de vin’ and mainly composed of shales and sandstones-pelites(Missenard et al. 2007). This basement rocks has formed under a low metamorphism degree and the major lineaments trend displays E - W and NE-SW direction (Mhamdi et al. 2017). Even if Cambrian outcrops of Marrakech High Atlas display strong volcanic activity (Michard, Ibouh, and Charrière 2011), lithostratigraphic analysis carried out by(Choubert and Faure-Muret 1962), shows that Cambrian series of Marrakech High Atlas give many similarities with other successions described in the Eastern Anti-Atlas (Ougnat). Afterward, Cambrian series were followed by Ordovician micro-conglomeratic and sandstone beds revealing a clearly regressive phase in the sedimentary evolution. The Continental deposits are overlain by anoxic black shales attributed to the Silurian period (Michard, Ibouh, and Charrière 2011)which are in turn overlain by Devonian silicoclastic rocks. (Choubert and Chazan 1957) describes a Carboniferous deltaic to turbiditc sequences in Marrakech High Atlas belt.

The Central and Northern parts of studied area are dominated by Mesozoic sedimentary cover, comprising several superposed sedimentary geological units, with the smaller outcrops of Paleogene to Neogene red mudstones in the south-eastern part of the study area (Fig.2). This overlying sedimentary cover includes some thicker formations of marine deposits and siliciclastic sediments ranging in age from the Permo-Trias to the upper Cretaceous. The Triassic deposits are mainly made up of red-bed facies and localized evaporates capped by extensive basaltic lava flows that are probably related to the initial rifting of the Atlantic Ocean (El Arabi et al. 2006). These syn-rift deposits(Perez et al. 2019),comprises fluvial conglomerate, siltstones and fine-grainedsandstones, that cover unconformably folded and eroded Paleozoic rocks. They outcrop in giant exposures West of Tighza where it occupies the borders of Tighza syncline. The basalt lava flows outcropped in the target area corresponds to the Central Atlantic Magmatic Province (CAMP), (El Arabi et al. 2006). Furthermore, they are associated with green marls that were palynologically dated Sinemurian (Courtinat and Algouti 1985). This data allowed dating Basalts formations from the Norian to the Hettangian (Biron and Courtinat 1982; Algouti 1991).

The Jurassic sedimentary succession is dominated by shallow-water sedimentation in the early Jurassic (carbonates and evaporates) that are detached over Triassic deposits(Saadi et al. 2011). The transition to Middle-Upper Liassic period is marked by the earlier change from carbonate to siliciclastic which is associated with appearance of evaporates and clay minerals and disappearance of carbonate facies. This continental clastic, mostly river, sediments includes mudstone and coarse-grained sandstone facies and has been classified into four stratigraphic units deposited in context of quiescent or active tectonic deformation(Cavallina et al. 2018)during Middle Jurassic (Saadi et al. 2011)or between Middle Jurassic and late Cretaceous time(Cavallina et al. 2018).

Concerning the cretaceous, it is represented by narrow outcrops exposed in the southern part of survey area (Fig.2). It is dominated by Cenomanian-Turonian shallow water carbonates related to the major transgression that covered North-West Africa (Leprêtre et al. 2018), followed by evaporitic redbed deposits of Coniacian to Paleocene continental period (Michard, Ibouh, and Charrière 2011). At last, the Quaternary sediments are the younger formation in the Telouet-Tighza inlier, where they are represented by floodplain terraces comprising mudstones, sandstones, as well as pebbles deposits (Fig.2).

From a structural point of view, this part of High Atlas belt is characterized by a thick-skinned structural style(Fekkak et al. 2018). The juxtaposition of Jurassic formations with intense fracturing basement makes this inlier a complex geomorphological domain (Fig.2). This geomorphology reveals that this area is intensively affected by many different tectonic phases as well as neotectonic movements. The majority of fractures appear in old basement where they dissect metamorphic rocks by NE-SW and sub-latitudinal trending faults(Ouanaimi 1989)(Fig.2). All major faults appearing in the northern part of geological map are linked to the west with the extended Tizi n' Test fault zone which is recognized as deep thrust in the western basement of Marrakech High Atlas belt (Fekkak et al. 2018; El Arabi et al. 2006)describes Triassic synsedimentary basins controlled by NE to E normal faults especially around to Telouet village. These structures are resulted from the reactivation of inherited Variscan fractures in double extension context during Middle Anisian (El Arabi et al. 2006). Paleogeographic studies of this region reveal that deposition of Liassic series was also controlled by kinematic movements of the same faults (Algouti, 1989) that are probably attached to the west to the giant south Atlasic fault (Saddiqi, Baidder, and Michard 2011). Therefore, the south Atlasic fault outcrop southeast of Tiliouine (Fig. 2) as a steep reverse fault whereas it disappears westward under Mesozoic-Cenozoic cover of Adrar Aglagal fold (Leprêtre et al. 2018);(Cavallina et al. 2018). However, (Domènech et al. 2015)suggest that not all fractures of south Atlasic fault zone and Tizi n' Test fault zone have being played as a reverse faults during the Cenozoic inversion event.

The study area displays diverse and complex topography (Fig 1C and 3A) probably caused by long geological and tectonic evolution. The elevation of the investigated area ranges between 0 to 3600m(Fig. 3A and 3C). The 3D view of Digital Elevation Model as well as the trend of topographic profile (Figs. 3A and 3B) carried out in studied area showed globally increase from west to east with maximum altitude of 3600m. The Telouet region topography is characterized by very low inclined structures expressed in the topography by large carbonate plateaus called 'Khela plateaus' whereas the East part of Tighzafold shows rugged topography with mountains piling up and areas of almost flat topography (Figs. 3A and 3B). In this region, the upper Jurassic to lower Cretaceous lithostratigraphic units form high-relief rugged morphologies that are organized to the east into acute anticlinal and large synclinal depressions. In flat topographic areas the fracture-related to topographic features are ambiguous. However, a sudden change in topography manifested by slope and ridge is identified in many areas.In the second topographic profile (Figs. 3C) oriented NW-SE (Figs. 3A), the altitudinal contrasts coincide perfectly with the major faults of Telouet –Tighza area. In addition, previous studies showed that topographic profiles can be used to reveal the presence of faults faults(Abdelkareem et al. 2021).The E to NE trend of landscape pattern especially in eastern part of targeting area reflects a marked structural control of topography by faults (Figs. 3A). In general, there is a close relationship between geological lineaments and topographic relief; several faults form clear topographic features that appear in the lineament map. It is common that the abrupt changes in topography might be the consequence or the outcome of structural phenomena such as, faults, joint sets, folds or fractures (Epuh et al. 2020). Accordingly, detailed extraction of topographic features will help in identifying lineaments and interpreting the tectonic history of this region. Notably, 3D maps generated from SRTM DEM data (Figs. 3A) were used here because they allow visualizing the morphology of the reliefs and tending to highlight the topographic contrast. Furthermore, 3D maps products were employed to understand geomorphological characteristics of Telouet-Tighza area and validate lineaments automatically extracted.

3. Data-sets

3.1. Geologic map

The geological map (Fig. 2) used in this study was extracted from geological map of Morocco published by the Geological Survey of Morocco. This map includes several sheets covering the entire national territory at1:1000000 scale. The region benefits from a few geological studies and most of them are focused in stratigraphic and lithostratigraphic topics lithostratigraphic topics (Courtinat and Algouti 1985; Cavallina et al. 2018). Structural analysis studies of this region are generally scarce and fragmentary; most works mention this area by synthetic descriptions.

For the current study we prepared a subset (Fig. 2) (258.449 ha) from this geological and geomorphological map by digitizing manually various lithostratigraphic units and major fracture networks characterizing the targeted area. The manual extraction of faults from geological map used in present

work is a primordial step. A total number of 26 structural lineaments ranging in size from 3, 4 Km to 66, 46 km were manually extracted from geological map (Fig 4A and 4B). The analysis of the length of geological lineaments digitized from local geological map reveals that the total length of major faults is 467,79km (Fig 4A). The Rose Diagram of these major faults constructed by using GIS tools show two dominant directions of ENE-WSW and E-W (Fig. 4C). Fig. 4A shows a general view of structural lineaments digitized from geological map of the study area. This fault map was used as a reference for defining structural features of a deformed field area and it was used as an appropriate benchmark for confront the resulted lineaments and assessing the validity of our final resulting product. Previous studies showed that geological map was a power tool used to eliminate non geological features.

3.2. Landsat Data

Recently launched in February 2013, Landsat-8 is the new generation of the series of Landsat satellites. It has the highest temporal repetition of earth observations from the Landsat series; currently it acquires images of scene every 8 days. Moreover, The Landsat-8 provides acquired data with high radiometric resolution and better signal - noise performance as well as the scenes cover is about 185 x 180 km (Adiri et al. 2016). As a form, Landsat-8 is a free-flyer spacecraft carrying two instruments, the Operational Land Imager (OLI) and the Thermal Infrared Sensor (TIRS), which collect image data in 9 and 2 bands respectively. The first sensor is OLI (Operational Land Imager) with 8 bands of 30 m in spatial resolution (Table 1): 1 band of cirrus (1.36 to 1.38 µm), 4 in the Visible (VIS) (0.43 to 0.67 µm), 2 bands of the Shortwave Infrared (SWIR) (1.57 to 2.29 µm) and 1 band of the Near Infrared (NIR) (0.85 to 0.88 µm). Moreover, it has a panchromatic band (0.50 to 0.68 µm) with 15 m in spatial resolution. While the second sensor namely TIRS (Thermal Infrared Sensor) is characterized by 2 spectral bands of 100 m in spatial resolution. The performance characteristics of OLI sensor are shown in Table 1. We processed two Landsat-8 OLI scenes acquired respectively on 09 July 2016 and on 28 August 2020 under excellent weather conditions, with 0% cloud cover for the entire scene. These cloud-free level 1T (corrected terrain) Landsat-8/ OLI images are provided by the United States Geological Survey (http://earthexplorer.usgs.gov), with a Universal Transverse Mercator (UTM) projection considering the World Geodetic System WGS 84 datum.

3.2. Radar data

The methodology used in the present study consisted to integrating SRTM digital elevation model (DEM), which yields geological, geomorphological and structural information below the surface, for terrain characterization (Abdelkareem et al. 2021). SRTM was a mission of 11-day performed by single-pass satellite (SAR interferometry) during February 2000 (Okeke, Ukaegbu, and Egesi 2019).The Spaceborne Imaging Radar hardware, which provides high quality elevation values, formed the SRTM instrument (Han et al. 2018).In several studies, radar remotely sensed SRTM data has proved to be extremely effective for many applications (Elmahdy, Mohamed, and Ali 2021) especially for highlighting geologic structures and fractures controlled by topography (Shandini et al. 2020; Abdelkareem et al. 2021). It affords a lot of advantages giving a great help in geological and geomorphological mapping which enables the interpretation of regional tectonic morphology(Han et al. 2018).The SRTM Digital Elevation Model is used in this study to derive shaded relief images as well as three-dimensional representation of the terrain and slope. Products generated from SRTM-DEM of the area were applied to derive average elevation of the terrain and detect a large number of lineaments, not identified before in optical images (Xu et al. 2020).Multispectral images may give a 'false edge' caused by noise, cloud cover, attitude of the satellite and illumination conditions (Han et al. 2018).All these factors reveal that become necessary to implement another spaceborne satellite product to automatically extract significant geologic features and analyze the tectonic evolution of survey region. The fact that DEM data are not affected by weathering or other factors, their high precision and their ability to represent the vertical extension of the earth's surface explains its extensive use during recent years(Elmahdy, Mohamed, and Ali 2021).In addition, experts now tend to use DEM data to extract geologic lineaments especially for highly vegetated terrains (Cirés et al. 1997). SRTM image freely download from the website http://search.asf.alaska.edu. ,has been acquired on June 06 2021 at 11:17 UT with 12 m in spatial resolution.

Table 1: Characteristics of the OLI sensor.

Subsystem of Landsat 8-Oli	VNIR	SWIR	VNIR	
Spectral range	Coastal aerosol (0.43-0.45) Blue (0.45-0.51) Green (0.53-0.59 Red (0.64-0.67) Near Infrared (0.85-0.88)	Shortwave Infrared (1) (1.57-1.65) Shortwave Infrared (2) (2.11-2.29)	Panchromatic (0.50-0.68)	Cirrus (1.36-1.38)
Spatial Resolution	30m	30m	15m	30m
Spectral Resolution		9bands		
Radiometric Resolution		16 bits		
Swath Width		185 Km		

4. Methodology

The Two OLI images were radiometrically calibrated, and then atmospherically corrected. Accordingly, the raw data in digital numbers of Landsat-8 OLI image bands were converted to the radiance. Then, both images were corrected for additive and multiplicative atmospheric effects by using FLAASH Model

embedded in the ENVI software (Fast Line-of-sight Atmospheric Analysis of Spectral Hypercubes) and by Applying the Dark Object Subtraction (DOS) method (Adiri et al. 2016). FLAASH module, which remove the molecular and particulate scattering, was qualified by Previous studies to be valid and efficient for preprocessing multi-spectral imagery (Ye et al. 2017). According to these studies, it allows obtaining spatially and radiometrically corrected images and consequently achieving the main purposes of the study.

In addition, a digital elevation model (DEM) derived from SRTM was considered in this study. The mosaicked Landsat scene and SRTM image were both later clipped to the extent of the targeting area for processing methods. The studied area clipped from a mosaic of the two preprocessed Landsat images has been further subjected to image enhancement techniques such as BR, PCA and DF. These techniques aim to yield more contrasting bands and reduce image noise. Furthermore, the optimum index factor (OIF) was applied to select the best RGB band composite images based on standard deviation and correlation coefficients. Afterwards, automatic lineament method was applied on SRTM shaded relief as well as on the raster obtained from the directional filter of selected CCB and PCA images. Resulted products are then checked and validated by overlapping withBR image selected and faults digitized from local geological map in order to discard lineaments of entropic origin. Last step consists to compute the orientation and the length of structural features as well as verify and validate extracted lineaments by using digitized geological map so as to construct a new lineament map. The flow chart of the methodology, adopted in Landsat image and SRTM shaded relief processing for extracting the meaningful lineaments in the study area, is shown in Fig. 5.

5. Processing

5.1. Principal Component Analysis

PCA is a multivariate statistical technique (Al-Djazouli et al. 2019), as well as a mathematical procedure, introduced by(Pearson 1901), which allow by orthogonal linear transformation to reduce a large set of data and to transform a number of (possibly) correlated variables into a (smaller) number of uncorrelated new variables called Principal Components (Hermi et al. 2017). Consequently, this transformation removes the irradiance and the redundancy effects of the satellite data(Amer, Kusky, and Ghulam 2010), isolates noise, extracts the most information present in the different bands, maximizes the amount of variance of the input data and then improves the targeted information in the image (Hermi et al. 2017; Abdelouhed, Ahmed, Abdellah, and Mohammed 2021; Abdelouhed, Algouti, et al. 2021). PCA is an efficient technique widely used for identification of lineaments due to its advantage for dimensionality reduction and enhancing multispectral image(Yu et al. 2012; Adiri et al. 2017; Al-Djazouli et al. 2019). Some of these studies have achievedlineament mapping by applying Principle Component analysis method on Landsat 8-Oli multispectral data in order to enhance the structural features(Salui 2018; Farahbakhsh et al. 2020; Aretouyap et al. 2020; Arifin, Adnan, and Rasam 2021; Nedjraoui et al. 2021)

Here, PCA is used to reduce data and to enhance the contrast of the image in order to determine the best principal component of Landsat 8 OLI for extracting lineaments in the Telouet –Tighza area. Six bands of the Principal Components (PCs) were derived from the mosaic of two Landsat8-Oli multispectral images covering the study region. The six principal components obtained are represented in Table 2 with their statistical calculations. The statistical calculations of the resulted Principal Components (PCs) showed that the first component synthesizes around 96% of the original information which mean that this component seems indispensable. The other components seem unnecessary because it contain each one less than 3% of information and decrease in turn. This criterion justifies the choice of the PC1 for the extraction of lineaments and its use to precise the initial structural map in this study. Linear features and edges are better visible and clear on the first principal component PC1 (Fig.6) than on the original mosaic.

5.2. Spectral Band Color Compositions

Multispectral images are often displayed as (RGB) color composites using three spectral bands (Hamdani and Baali 2019). Several studies used composite bands in lineament mapping; different (RGB) color composition were combined through selected bands and then every three combinations bands of spectral bands were examined in order to determine the most combination containing the high amount of information when combined in a composite image (Mhamdi et al. 2017; Aldharab et al. 2018; Farahbakhsh et al. 2020).

OIF is a selection method developed by (Chavez, GL, and LB 1982) which allow selecting the bands containing most of the variance and then to optimally display Landsat 8 data in three color composite images. There are many examples of studies that used OIF technique as a preliminary processing step before the automatic extraction of lineaments (Al-Djazouli et al. 2019; Jellouli et al. 2021). This technique of enhancement, which is often used to better visualize the boundaries between lithological units, was calculated by the following formula (1):

$$OIF = \Sigma(\text{Standard deviation } (i, j, k) / \Sigma (CC (i, j), CC (i, k), CC (k, j)) \quad (1)$$

i: the first selected band

j: the second selected band

k: the third selected band

CC: Correlation coefficient of each couple of bands

In this study we suggest the use of the optimum index factor (OIF) and correlation index to select the best independent band combination useful to achieve the aim of this study. The band combination which has the lowest correlation and highest variance among band pairs is the best one. the 7 Landsat-Oli bands image have been processed using Ilwis 3.3 software and indicated that 6-5- 7 band combination has the highest sum of standard deviations and low level of information redundancy (table 3).). (Jellouli et al. 2021)suggest the choosing of the three bands with the highest variance because they combine the largest amount of information (high optimum index factor, OIF). In the other hand statistics calculation of PCA provided the correlation matrix shown in table 4. In an

effort to improve lineament extraction of this study, we selected the 6-5-7 three bands that present the highest OIF (table 3) whereas the other four bands are eliminated. Furthermore, these same bands display the least amount of duplication (low correlation index see table 4) what's means that they should give the best lineament mapping. The selected bands are then displayed in red, green and blue to create a colored combination image. The colorful image composed of the three selected bands is shown in Fig. 7 with high visual quality. Beside the geological formations, hydrographic network and vegetation, the chosen compositions composite (RGB) image highlight the most structural information preserved in all bands and display the clearest linear geostructures which were subsequently extracted by automatic method.

Table 2: Statistics of Principal Component Analysis of the used Data set

PC bands	EigenValue	Percentage %	Accumulative Percentage %
1	108346304,33	95,21	95,21
2	3378111,90	2,96	98,18
3	1455480,49	1,27	99,45
4	367148,58	0,32	99,78
5	208317,32	0,18	99,96
6	36794,21	0,03	99,99
7	2583,84	0,0023	100

Table 3: Statistics of OIF analysis applied to the seven OLI bands.

Option/ Combinaison	OIF Highest Index Ranking			Percent
1	B	B6	B7	88,96
2	B4	B5	B6	83,54
3	B4	B6	B7	81,99
4	B3	B5	B6	90,12
5	B4	B5	B7	79,63
6	B1	B5	B6	79,62

Table 4: Matrix of correlation index derived from PCA analysis of the seven OLI bands.

Bands	1	2	3	4	5	6	7
1	1,00000	0,99433	0,95697	0,88663	0,88426	0,95107	0,92914
2	0,99433	1,00000	0,98119	0,92415	0,90864	0,87059	0,86737
3	0,95697	0,98119	1,00000	0,97407	0,94007	0,93414	0,92953
4	0,88663	0,92415	0,97407	1,00000	0,94185	0,96859	0,97273
5	0,88426	0,90864	0,94007	0,94185	1,00000	*0,82842*	*0,82633*
6	0,95107	0,87059	0,93414	0,96859	0,82842	1,00000	*0,80018*
7	0,92914	0,86737	0,92953	0,97273	0,82633	0,80018	1,00000

5.3. Band Ratios

Because of their proven ability to enhance the lithological discontinuities which can indicate the presence of lineaments (Hamdani and Baali 2019), different band ratios of Landsat 8- Oli data were used extensively for lithological and lineament mapping in many geological environments, depending on the purpose of the study (Abdelkareem et al. 2021; Saidi et al. 2020). Githenya, Kariuki, and Waswa (2019), deduced that Landsat 8 performed at discriminating structural features using 7/5, 6/4, 4/2 band ratios, while Kolawole (2016)used Color bands ratio of 5/6, 5/4, 4/1 to extract structural lineaments in North Central part of Nigeria. In addition, Hamdani and Baali (2019)showed that Landsat 8-Oli data have important potential for mapping geological lineament, related with karst shapes, by applying band ratios 6/ 7, 3/ 4, 5/ 6 in Moroccan Middle Atlas.

The band ratiois an arithmetical operation used to enhance the spectral differences between bands. Exploiting the variation of reflectance in the spectral signature, this image processing technique consists of dividing Digital Number (DN) of one spectral band by DN values of another one in a multispectral scene (Githenya, Kariuki, and Waswa 2019). In other wise it allows to reduce haze and vegetation cover, to suppress the topographic slope and minimize shadow effects, particularly in mountainous areas where shadow is one of the major problems in satellite imaging (Kolawole et al. 2016).

Based on the results of PCA transformation and OIF compute, it is evident that the Landsat 8-OLI band-ratio image 6/7-6/5-3/2 (Fig. 8) is powerful in distinguishing the lithological boundaries and edges in the study area. Then, it is used as powerful tool to check and validate extracted lineament, eliminate lineaments corresponding to lithological boundaries and distinct structurally significant lineaments.

5.4. Directional Filter

Directional filtering is defined as a spatial domain filtering (Javhar et al. 2019),Thataccentuates the first derivative between each two adjacent pixels and selectively bring out any feature in the input image having specific direction gradients (Epuh et al. 2020; Jellouli et al. 2021). It consists of changing the values of pixels by replacing each center pixel by the median value within the neighborhood pixels (Farahbakhsh et al. 2020). The resulted image comprises pixels with uniform values while the others present variable values that indicate bright edges (Epuh et al. 2020). Furthermore, the directional nature of structural lineaments give up to the obligation of using directional filtering in order to enhance the perception of the structural features when processing multispectrales images (Javhar et al. 2019; Hermi et al. 2017) displayed in his study that the directional contrast gradient is produced by filtering algorithm on the input image independently of lineaments orientation. It can detect structural lines with horizontal, vertical, and diagonal directions(Hermi et al. 2017). Directional filters were commonly used by several authors in geological applications to enhance and highlight specific linear trends as well as geological (Hermi et al. 2017; Abdelouhed, Ahmed, Abdellah, and Mohammed 2021; Abdelouhed, Algouti, et al. 2021).In the present study, the DF technique was selected for the automatic lineament extraction, since it is considered such a faster and effective way to evaluate lineaments and identify any linear or curvilinear shapes (faults, fractures, contours, roads and defects...) on the image (Nedjraoui et al. 2021; Azman, Ab Talib, and Sokiman 2020). This straightforward method allows the enhancement of lineaments in study area using the Sobel operator(Sedrette and Rebai 2016). This latter is a variety of directional filters where the values of the convolution matrix depend mainly on the distance from the central pixel. Edge enhancing filter is used for detailed identification of lineaments and highlighting any changes of gradient, that are not promoted by the illumination source, by causing an optical effect of shadow on the image as if it were illuminated by oblique light shadow ((Hamdani and Baali , 2019;Azman, Ab Talib, and Sokiman 2020). Accordingly, it is applied to reduce noise and smooth the image ((Bentahar, Raji, and Si Mhamdi 2020; Singh, Arya, and Agarwal 2020).In order to enhance the geological lineaments in all directions, four derived images have been generated from four directional 5x5 Sobel filters in the four principal directions: N-S, E-W, NE-SW and NW-SE (Table 5). This step is performed by applying the directional convolution filter on PC1 and on the selected color composite image (6-5- 7 RGB) via Envi 5.2 software. In addition, the use of the PC1 and 6-5- 7 image is justified as they contain a large amount of information that is manifested by showing most of the features and enhancing linear geological structures in terms of high spectral resolution and contrast. The size of the filters is determined according to the size of the fieldwork; 7x7 matrix kernel size selected in this study would take into consideration all lineaments with small length (Aretouyap et al. 2020). Table 5 display the size and weight of kernels applied in the study area. The outputs resulted from directional filtering of PC1 and 6-5- 7 images are shown respectively in Fig. 9 and Fig.10.

Table 5: Convolution matrix of different directional 7*7 filters.

N0							**N45**					
-1.0000	-1.0000	-1.0000	0.0000	1.0000	1.0000	1.0000	-1.4142	-1.4142	-1.4142	-0.7071	0.0000	0.0000
-1.0000	-1.0000	-1.0000	0.0000	1.0000	1.0000	1.0000	-1.4142	-1.4142	-1.4142	-0.7071	0.0000	0.0000
-1.0000	-1.0000	-1.0000	0.0000	1.0000	1.0000	1.0000	-1.4142	-1.4142	-1.4142	-0.7071	0.0000	0.0000
-1.0000	-1.0000	-1.0000	0.0000	1.0000	1.0000	1.0000	-0.7071	-0.7071	-0.7071	0.0000	0.7071	0.7071
-1.0000	-1.0000	-1.0000	0.0000	1.0000	1.0000	1.0000	0.0000	0.0000	0.0000	0.7071	1.4142	1.4142
-1.0000	-1.0000	-1.0000	0.0000	1.0000	1.0000	1.0000	0.0000	0.0000	0.0000	0.7071	1.4142	1.4142
-1.0000	-1.0000	-1.0000	0.0000	1.0000	1.0000	1.0000	0.0000	0.0000	0.0000	0.7071	1.4142	1.4142
N90							**N135**					
-1.0000	-1.0000	-1.0000	-1.0000	-1.0000	-1.0000	-1.0000	0.0000	0.0000	0.0000	-0.7071	-1.4142	-1.4142
-1.0000	-1.0000	-1.0000	-1.0000	-1.0000	-1.0000	-1.0000	0.0000	0.0000	0.0000	-0.7071	-1.4142	-1.4142
-1.0000	-1.0000	-1.0000	-1.0000	-1.0000	-1.0000	-1.0000	0.0000	0.0000	0.0000	-0.7071	-1.4142	-1.4142
0.0000	0.0000	0.0000	0.0000	-0.0000	-0.0000	-0.0000	0.7071	0.7071	0.7071	0.0000	-0.7071	-0.7071
1.0000	1.0000	1.0000	1.0000	1.0000	1.0000	1.0000	1.4142	1.4142	1.4142	0.7071	0.0000	0.0000
1.0000	1.0000	1.0000	1.0000	1.0000	1.0000	1.0000	1.4142	1.4142	1.4142	0.7071	0.0000	0.0000
1.0000	1.0000	1.0000	1.0000	1.0000	1.0000	1.0000	1.4142	1.4142	1.4142	0.7071	0.0000	0.0000

5.5. Shading relief

The DEM data can be obtained from various remote sensing sources such as ASTER (30 x 30 m) and SRTM (90 x 90m global DEM). In this study, we used SRTM data acquired with the radar C-band at 3 arc second (12 m in resolution), from the Consortium Space Information(Masoud and Koike 2006). SRTM digital elevation model is frequently used to automatically extract the structural features as well as to improve the quality of lineament map by its spectral and resolution properties. In the current study, shaded relief images generated from SRTM digital elevation model will enable the easy recognizing of geological lineaments and evaluating the structural implication of the lineaments resulted from processing of Landsat 8 Oli image. Using ArcGIS 10.2, shaded relief images were produced from SRTM digital elevation model by applying Analytical hill-shading. This latter is used as a common method useful to simulates the topographic illumination under different artificial light directions by introducing both altitude and azimuth parameters(Abdelouhed, Ahmed, Abdellah, Mohammed, et al. 2021). Therefore, this new technique becomes necessary to automatically extract and analyze geologic lineaments using a combination of DEM and remote sensing images. Several studies utilizedshaded relief for the extraction of lineaments and have showed that this can be used as a powerful

tool to explore and improve lineament mapping in mountainous areas due to its ability to simulate shadow effects that are provoked by the sun angle and elevation (Saadi et al. 2011)

This step involves selecting some parameters that are necessary for better discrimination between shaded and illuminated areas, namely the azimuth and the altitude angle(Jellouli et al. 2021).

Maintaining solar illumination angle at 30°, four shaded reliefs were created with four contrasting illumination directions 0°, 45°, 90°, and 135° (Fig. 11). According to (Bentahar, Raji, and Mhamdi 2020; Farah, Algouti, Algouti, Errami, et al. 2021; Farah, Algouti, Algouti, Ifkirne, et al. 2021), the boundaries between the shaded and unshaded ground areas show the presence of lineaments that should be validated by using control geological field map.

5.6. Slope

The synergistic use of slope parameter for validation of detected lineament was proposed in many lineaments mapping studies (Abdelouhed, Ahmed, Abdellah, Mohammed, et al. 2021; Adiri et al. 2017; Jellouli et al. 2021).Because of its Availability as an under product easily extractable from digital model data and its higher spectral resolution, slope data appears as important parameter in lineament studies. In this work, the slope derived from SRTM digital elevation model (12m resolution) is performed as an important tool to highlight the Abrupt changes in slope values which are often a key indicator for detecting linear structures(Jellouli et al. 2021). Furthermore, perhaps most importantly, high values in the slope are commonly considered as probable lineaments because they suggest steep slopes.

5.7. Automatic lineaments extraction

In the present work, the automated lineament extraction was involved by using the most broadly used module LINE extraction of PCI Geomatica version 2016 software. The algorithm was designed to detect lineaments from both radar and optical images because of its many advantages in the automatic extraction of lineaments such as: less time-consuming and high ability to extract the linear segments and features when it is compared with manual extraction method (Aldharab et al. 2018).

The process of automatic extraction of lineaments consists of three stages, namely, edge (contours) detection, thresholding and curve extraction (Epuh et al. 2020; Shandini et al. 2020).The edges detection filter identifies the limits of abrupt changes in the values of neighboring pixels (Jellouli et al. 2021).In the second step, PCI Geomatica software detects successively lines which often refer to lineaments. Furthermore, various optional parameters (RADI, GTHR, LTHR, FTHR, ATHR and DTHR) defined by users, control automatic extraction of the lineament process with a view to enhance resulted data (Aretouyap et al. 2020).The selection by users of these parameters values depend mainly on spatial image resolution, lineament density and type of used data (Thannoun et al. 2013).These six parameters must be added simultaneously to LINE module of Geomatica in order to extract lineaments from radar or optical image and then to convert these polylines in vector form (Ibrahim and Mutua 2014). The six parameters used in this are briefly explained in Table 6.

The automatic lineaments extraction was carried out in this paper by involving two steps: the first step consists to select the optimal band from the available datasets (Landsat 8 and STRM DEM) that should be used for automatic lineament extraction. The optimal inputs were tested to select the most suitable input which presents the high ability to identify the linear features over the study area. For more enhancements, the input in this study was the four directional filter (N0°, N45°, N90°, and N135°) generated from the derivatives of the mosaicked OLI images (including 6-5-7 color compositions and PC1 neo component). According to Abdelouhed, Ahmed, Abdellah, Mohammed, et al. 2021, the first principal component image and color composite bands are useful for discrimination of lineaments and delineation of geological features because lineaments are well interpreted in this data. Subsequently, line model was applied to the four shaded relief (N0°, N45°, N90°, and N135°) created from SRTM DEM (with a ground resolution of 12 m) so as to increase the visibility of small features. In the second step, the necessary and appropriate LINE module parameters should be selected through several setting tests and visual inspections of the output in order to get the most credible lineaments related to the tectonic setting of the study area. Since the numbers and lengths of geologic lineaments automatically extracted by this module depends on the values of the input parameters(Aretouyap et al. 2020)different combinations of parameter values provided by literature and ground truth are evaluated in order to select the optimal LINE values that produced a satisfactory result of the lineaments extracted (Saidi et al. 2020).After adjusting the parameters and assessing the outputs, combination of settings values, that gave the reliable and the more appropriate lineament results, was selected. The default values and the values of parameters adopted in this work are provided in Table 7.

After extraction, the lineaments resulted from different input data were converted to Arcgis shapefile format. The sum of lineament automatically extracted from different data-inputs is about 12.283. The Data extracted reveals structural lineaments that were later confirmed by comparing with the corresponding ancillary data.

Table 6: The Parameters of the LINE module.

Step	Parameters	Significations	Range and Units
Contours detection	RADI (Filter radius)	Specifies the radius (in pixels)that will be used in edges detection filter in order to use the lower values to detect more details and high values to minimize noise detection. This parameter roughly defines the small detail in the processed image to be detected values between 3 and 8 are acceptable	0-8192 (Pixels)
	GTHR (Gradient threshold)	This parameter specifies the threshold of brightness change and it is defined as a minimum value of gradient that can be considered as an edge during the edge detection	0-255 (Unitless)
Line detection	LTHR (Length threshold)	It expounds the minimum length of curve (in pixels) used for mapping curved linear objects THAT are taken as the lineament for further consideration (a value of 10 is suitable)	0-8192 (Pixels)
	FTHR (Line fitting error threshold)	specifies the tolerance allowed when fitting arc or line segment to form a (curved) lineament Values between 2 and 5 are ideal	0-8192 (Pixels)
	ATHR (Angular difference threshold)	Defines the maximum angle(in degrees) not to be exceeded between two neighboring polyline to be linked Values between 3 and 20 are recommended	0-90 (Degree)
	DTHR (Linking distance threshold)	this measurement specifies the minimum distance (in pixels) between the endpoints of a polyline to be linked Values between 10 and 45 are suitable	0-8192 (Pixels)

Table 7: The defaults and the applied values of line-module parameters that are used in this study.

Line Module Parameters and Units		Default Values	Used Values
1. **RADI (Pixels)**		10	25
2	**GTHR (0,225)**	100	90
3	**LTHR (Pixels)**	30	50
4	**FTHR (Pixels)**	3	7
5	**ATHR (Degrees)**	30	40
6	**DHTR (Pixels)**	20	30

6. Control And Validation

Post-processing is a necessary step for check and validation that aims to discard non geologic lineaments and prevent unnecessary extraction of linear shapes(A. et al. 2020; Farah, Algouti, Algouti, Errami, et al. 2021; Abdelouhed, Ahmed, Abdellah, Mohammed, et al. 2021; Adiri et al. 2017; Jellouli et al. 2021). The Automatic process used in this work has created high amount (in total about 12.283) of lineaments; all linear and curvilinear features, without any distinction are identified. However, According to (Jellouli et al. 2021), many lineaments derived from remote sensing data by applying the automatic methods are insignificant and without any geological importance. Consequently, it is necessary through careful checking of resulted lineaments, to identify non-geological lineaments and detect features not generated by faulting(Arifin, Adnan, and Rasam 2021). Lineament are a linear structures or curvilinear edges that may correspond to geological structures (faults, joints, lithological boundaries and other line weaknesses), geomorphological features (cliffs, linear valleys and terraces), tonal contrasts linked to vegetation and anthropogenic features (tracks, roads and electric grids) (Aretouyap et al. 2020).These latter are generated by several kinds of human activities and act as a noise masking structural information and making the perception of geological lineaments very difficult (Hermi et al. 2017).

In the present work, we are interested only for the structural lineaments, hence every meaningless lineament related to different parameters (subset boundary, road, track, ridge line, River, shade, cultivated areas etc.) is removed by using GIS tools. Fig 12 A and 12B displays some examples of non-geological lineaments that correspond respectively to hydrographic network, edges and roads. This task is accomplished by superimposing lineaments extracted from each azimuth angle to bibliographic data (high resolution Google Earth images, topographic and geological maps of Telouet-Tighza area), the linear features in shapefile format were edited in ArcGIS 10.2 software in order to eliminate excessive line clutters and distinct structurally significant lineaments related to the tectonic setting. Digital elevation map overlapped by the lineaments pattern has also served to detect and remove false hits of lineaments and then to avoid their extraction. In addition, the band ratio composite 6/7-6/5-3/2 were used as reference points to highlight the lithological boundaries. The selected band ratio image (Fig. 8)has the advantage of discriminating different lithological units in various colors as well as preserving morphological features because the high information within used bands. The extracted lineaments displaying a trend analogous to well-defined lithological boundaries are visually removed which reflect the usefully of band ratio technique for validation of linear structures. Fig 12 C displays example of extracted lineaments correspondent to lithological boundaries.

Another tool for validating resulted lineaments is a field works. Our field mission consisted mainly in checking lineaments extracted by visiting several places as shown in Figure 13.A precise observation of the faults and boundaries facies already existing on the old geological map, contributes to update the new map realized in this work. The field mission allowed us to better improve the present study by discarding nonstructural lineaments.

After control and validation, the rest of lineaments extracted in the four directions from each image processing data were merged to form tree composites lineaments maps of the study area. These lineaments maps elaborated and their statistical analysis, are shown in figures 14, 15 and 16. This analysis assured that obtained lineament maps have been properly controlled and validated.

7. Results And Discussion

7.1. Statistical analysis

7.1.1. Orientation and length frequency

Several works show the use of statistical analyses of lineaments for studying the geometry of lineament networks and recognizing the dominant directions as well as morphotectonic condition at a regional scale. Statistical analysis aims to determine numbers, lengths, densities and trends of extractedlineaments. These Geometric parameters play a huge role in the structural description and provide basic information to understand and interpret the striking faults as well as the tectonic evolution of the studied area. The lineament length distribution is achieved by creating length frequency histogram for each of the extracted lineaments as well as the existing faults digitized from geological map of the study area (Fig 4, 14, 15 and 16). In this step, the compute of geometric parameters was performed by means of Arc GIS 10.2.2 software.Applying the automatic extraction processing has produced a large number of extracted lineaments. Two synthetic maps were elaborated by combining lineaments extracted in the four directions from PC1 OLI and 6-5-7 band composite OLI image. The third lineament map was constructed from SRTM shaded relief images. All maps were firstly edited and validated, and then the resulted maps and their statistical analyses are shown in Fig. 14, 15 and 16.

As shown in the Fig.14 and 15, the PC1 OLI image and 6-5-7 RGB OLI image provided a large number of extracted lineaments in order of 680 and 1691 respectively. This underlines the adequacy of extracting lineaments from any multiple azimuth angles.

Even if SRTM shaded relief image displayed the highest number of extracted lineaments, some of these lineaments are relatively insignificant. The maximum length of the lineaments extracted in this paper is 15.13 km which is provided by PC1 analysis (Fig.14B). The values of the lineament length corresponding to the PC1 Landsat 8-OLI image range from 2,5 km to a maximum of 15,13 km with the majority of the extracted lineaments between 3 km and 3,5 km long (Fig. 14 B and 14 C). These values show that the large number of lineaments extracted from PC1 image are very long. The values show a range between 60 m and around 11, 9 km for the 6-5-7 color composite OLI image (Fig. 15B), with an average length of 2, 9 km while the values of lineaments length for the SRTM shaded relief image (Fig. 16B and 16C) show the same dominance of the low values of length. The length of the major part of lineaments extracted from SRTM data range between 1 and 1, 8 km. In order to compare the lineaments extracted from different data used in this study, the number and length of extracted lineaments is displayed in table 8. The total length of lineaments extracted from OLI sensor's PC1 and 6-5-7 CC is respectively 3231 km and 3541 km, which is slightly lesser than the total length (4416 km) of the SRTM-DEM output. From the statistical descriptions, it can be seen that the selected bands composite (6-5-7) image (Fig. 15A) extracted more lineaments compared to the PC1 image (Fig. 14A). Even if the lineaments extracted from the selected band combination are mostly concentrated in the boundaries between lithological formations, it shows additional details of lineaments (Fig. 15A), which were later compared with the local fault network. Furthermore, this statistical analysis showed that the lineaments extracted from the SRTM data show high spatial concentration (Fig. 16A) compared to those extracted from Landsat 8-OLI directional filter images (Fig. 14A and 15A) which mean that SRTM DEM gave the most significant result in lineament mapping among the other data source used in this work. A relatively high resolution of SRTM data explains its ability to clearly identify linear features. Several studies, mentions the highest performance of the radar data in extracting geological lineaments. Adiri et al. (2017)explains the good results of SRTM data in the lineament identification by its high sensitivity to geomorphology as opposed to optical data.

It can be noted that while SRTM shaded relief image provide high number of lineaments, structural features extracted from Landsat enhancement method through band combination and principal component analyses are also important and allows the better visualization and discrimination of some significant structures. This result is explained by the role of PCA as a good tool of data reduction and the role of directional filters in the perception of lineaments in all expected directions. The use of directional filters increases considerably the frequency and the number of the lineaments identified in this study.

Consequently, synergic use of Landsat 8- Oli and SRTM DEM images appears to be effective and useful because it shows the complementarity between these types of datasets. The SRTM DEM image allows the extraction of the smallest lineaments (Fig.16A), while Landsat 8 satellite is more robust in extracting longest structural lineaments (Fig. 14A and 15A). The high length of lineament detected from Landsat image compared with SRTM-shaded derived lineaments is explained by the higher spatial/ spectral resolution of Landsat data. The variation in statistical parameters of lineaments extracted from varied sources reveals the benefit of using many satellite images to map adequately the lineaments of this area.

In accuracy assessment, the orientation is another parameter broadly used in order to determine the most frequent directions in the extracted lineaments. After checking and editing, the DXF file of lineaments derived from Landsat and STRM images were imported into version Rockworks 16 software for the generation of rose diagrams. The Rockworks is a comprehensive program designed to derive lineament directions by offering rose diagram tool. All researches that are dealing with study of lineament features have usually employed Rose diagram to analyze lineament classification based on the number of the lineaments contributing to each orientation trend. The conventional method consists to produce the rose diagrams that determine the orientations of fractures by using end point of the coordinate of each line; despite its length (short or long), which allow the determination of structural features trend. Hence, the rose diagrams constructed show the distribution of fractures arranged by classes of 10° orientations. In addition, rose diagrams are used in this study in order to compare the orientation of lineaments extracted from the PC1, 6-5-7 and SRTM shaded relief images.The identified lineaments are subject to orientation analysis in order to highlight the main directions (Fig. 14D, 15D and 16D). The Fig. 14D shows that dominant direction of lineaments extracted from the PC1 Landsat image is ENE-WSW (N60-80 E), Whereas the rose diagrams (Fig. 15D and 16D) show that most of the lineaments extracted from the 6-5-7 Landsat 8 image, and SRTM data are trending E-W. However, the rose diagram of lineaments generated from SRTM data displays WNW-ESE as a second major trend (Fig. 16D). Generally,

the lineament maps (Fig. 14A, 15A and 16A) indicate a homogeneous distribution of lineament with an ascendancy of the lineaments of ENE-WSW trend. The three computed rose diagrams differ but point clearly to indicate this major trend with the remainder, less than 10%, which is oriented in different azimuth.

The different directional filters applied (N0, N45, N90 and N135) to further enhance the interpretation of the multispectral data showed similar results in the trend of lineaments extracted without significant change in predominant direction of ENE-WSW to NE-SW. Accordingly, the rose diagrams of the identified lineaments reveal similar preferential direction as shown in the geological map of Telouet-Tighza area (Fig.2 and Fig.4). This dominant orientation is in accordance with the direction of the major fault lines in Marrakech High Atlas belt. Therefore, these lineaments are highly concentrated in some parts of lineament maps and need to be compared with geological map in order to establish their probable correlation with faults existing in studied area. The North-West part of Telouet-Tighza area was found to have less frequency of lineaments in all tree processing runs. These results prove that satellites sources used in this work are preferred and suitable for lineament extraction of the studied area.

Table 8: Statistical results of the lineaments extracted from different data used in this work.

	PC1	6-5-7 CC	STRM
Number of lineaments	680	1691	2066
Minimum Length	2,453959	0,06	0,425184
Maximum Length	15,134589	11,935168	12,570836
Total Length	3231,924358	3541,752333	4416,661283
Mean Length	4,75283	2,094472	2,137784
Standard Deviation	1,770825	1,430795	1,019301

7.1.2. Line density

The density analysis is commonly used in combination with the statistical diagrams for lineament studies(Epuh et al. 2020; Shandini et al. 2020;Abdelouhed, Ahmed, Abdellah, Mohammed, et al. 2021; Jellouli et al. 2021).This statistical analysis method allows creating lineament density maps by using the line density tool embedded in the spatial analyst tool of ArcGIS 10.2 software environment. This tool computes the frequency of the lineaments per unit area which provide useful information about the spatial concentration of fractures. Therefore, it is adopted by many authors as an effective method for researching and then validating the lineament density distribution.

In the current work, density map is generated for characterizing the spatial patterns of lineaments in order to summarize and verify identified lineaments. Line density tool was applied separately on every lineament map (including overall lineaments of the four directions) in order to generate the lineament density maps of Landsat-derived lineaments and SRTM derived lineaments as well as the density map of overall faults and fractures in the study area. This latter map served for perception and comparison step. The produced maps are shown in (Fig. 17) by grids using natural break method.

The resulted density maps were used as an essential parameter to better correlate the spatial concentration of identified lineaments with the distribution of geological features in the study area (existing faults, lithological units). The superposition of faults manually digitized from geological map (Fig.4) with densities maps was used to find the relationships between the spatial density of lineament and the structures features of the target area.

Lineament density maps display that the high concentrations of lineaments occupied many parts of the study area. It reveals the existence of several fault zones in the area. The high-density values are remarkable next the major accidents of Telouet-Tighza area. In the Eastern part of the Telouet-Tighza area, there is a cluster of faults that are particularly identified in lineament density maps. These high densities are clearly adjacent to the major faults and correspond perfectly to the main faults.

The lineament density map of the PC1 image (Fig.17B) shows that fracturing is concentrated in the major faults at the Ait Tamlil village. Another high concentration appears next the major accident of Telouet (South High Atlasic faults) (Fig.17B). The lineament density map of the 6-5-7 image (Fig.17C) shows approximately similar results as the PC1density map; the same faults are highlighted by high values of densities. However, For the SRTM image (Fig.17D), the identified lineaments show small enclaves of high-density values within low densities, that display better high correlation with the most faults of the study area. In addition, all maps show high density that appears in the northwestern part of the area (at Tarast village) (Fig.17D) which is probably linked to an NE-SW fault zone not mapped bythe field work.

The low-density anomaly areas usually suggest a relatively stable tectonic rocks or Quaternary-covered area, whereas this irregular pattern in high density anomaly suggest being the result of high faulting processes in the area. Overall, the region was greatly influenced by tectonic faults that are highlighted here, with success, by high densities of lineaments automatically extracted.

7.2. Final Map

The synthesis lineaments map was produced by overlapping all segments obtained from the6-5-7 image, the PC1, and the SRTM shaded relief. The combination of the different results allowseliminating redundant/duplicate lineaments and merging SRTM lineament output with data products of Landsat 8 image into a single output. As nonstructural lineaments are already removed from all lineaments extracted, this output is considered as the final lineament output which undergoes statistical estimations (number and length of lineaments) by using Arc GIS software. The analysis of lineament Orientation was also performed by means of the Rockworks17 software.

In the next stage, the lineaments extracted from remote sensing data are compared and confronted with the major pre-existing faults on the geological map in view to give geological significance to the structural lineaments automatically extracted. Therefore, the main highlighted directions are compared to those of the geologic faults as well as their alignments and elongations. This stage of validation is necessary to evaluate qualitatively the relevance of the resulted output and the method performed, as well as to determine any possible relationship between the extracted lineaments and the structural geology of studied area.The synthetic map (Fig.18) shows 3242 widespread lineaments generated from the enhanced remote sensing data compared to only 26 digitalized from the local geological map. This comparison reveals that the number of lineament produced by remote sensing approach is greater more than the frequency of lineaments in the fault map (Fig.4) of the survey area. The second difference concerns the density of lineaments; the synthetic map displays some areas with high concentration of lineament while the thematic geological map shows wide distribution of faults. Another divergent point is that lineaments generated automatically are shorter than fault lines on geological map.The superposition of obtained results with faults digitized from geological map shows some similarities and suggests that geological map support the results obtained from processing of both Landsat 8-Oli and SRTM DEM images. Therefore, this superimposition reveals coherent results and show that the localization and the orientation of some lineaments converge very well with those of the existing faults in the targeting area. The coincidence of lineaments yielded from the processing of satellite images with the major fault directions prove the success of data and method used in this work to identify correctly some faults in the study area (Fig.18). The rose diagram of the different lineaments indicates two major families of orientations: NE-SW and E-W. Comparing these orientations with those of preexistent faults (Fig.4) indicates that both manually and automatically extracted lineaments present similar directions; they correspond perfectly to the dominant direction of the real faults. In addition, the synthetic structural map of lineaments allowed us to notice this result and suggest that the area is profoundly affected by these two structural trends. It can be inferred that the ENE-WSW and E-W dominant directions of lineament can be attributed to NW–SE and N–S regional extension directions respectively, that are recorded in Triassic deposits of this region as a normal faults(El Arabi et al. 2006). In addition,Ibouh et al. (2001) describes the same movement, in Liassic carbonates rocks, along Jbel Tizal-Azourki accident which is probably extended along the study area to confront the Tichka massif. Other authors suggest that this tectonic regime continue through all Jurassic period (Brahim et al. 2002). Both E-W and ENE-WSW trends are reactivated as reverse faults during Cenozoic shortening.

At the end, we conclude that Landsat 8 images combined with SRTM radar data can contribute fully to improve lineament mapping. In addition, a newly adopted automatic lineament analysis presented here significantly aid to extract precisely different lineaments. This technique offers a cost-efficient means in mapping structural lineaments in the studied area and in similar regions. The directional filtering algorithms used in this research prove their efficiency in highlighting lineaments in different directions.

7.2. Factors controlling lineaments distributions

7.2.1. Slope

For validating our results and understanding the spatial distribution of lineaments as well as geometry, and density map of fractures, we involve some factors (topographical factor and lithological factor) that are frequently used by several authors (Abdelouhed, Ahmed, Abdellah, Mohammed, et al. 2021; Jellouli et al. 2021)(Jellouli et al. 2021) to achieve the same aim. Slope images derived from SRTM DEM data are superimposed by lineaments identified from the Landsat 8 images (PC1 and 6-5-7) and SRTM data (Fig. 19 A, B and C). From the tree maps, the lineaments extracted from SRTM image show coherent results with slope map of the study area. The high values of slope, which express the change in elevation and suggest the occurrence of steep slopes, coincide very well with lineaments derived (Fig. 19C). This result supports the use of Radar images in mountainous areas with rugged terrain as an input data to extract lineaments (Abdelkareem et al. 2021). The highest sensitivity of the radar signal to topography and surface roughness explain the location of lineaments generated from SRTM image in areas with abrupt changes in slope values and very steep slopes.

7.2.2. Lithological Factor

After applying the lineament extraction process, the resulting lineaments should be superimposed on the geological map in order to understand their spatial distribution and their relation with tectonic setting. To accomplish this task, all lineaments extracted through processing of both SRTM DEM and OLI multispectral data are superposed on the lithological map extracted from the geological map of Telouet-Tighza inlier (Fig.20). The superposition aims to expose the lithological nature of terrains affected by fractures. From this superposition map, the concentration of lineaments shows a high value in several formations. However, the Paleozoic basement displays the highestdensity of lineaments. In term of hardness, the competent formations, which are represented by basement rocks including Precambrian and Paleozoic rocks beside Mesozoic carbonate, are affected by high number of lineaments(Fig.20). In addition, the most of the weak values (low densities) of lineaments are located in the Triassic tender units (like in the North of Telouet Village) and in the fragile Cretaceous rocks (Fig.20). This finding is not explained only by rheological behavior of these formations, but it involves also the orogenic impact of the regional tectonic (distance of structural lineaments from major faults). The Precambrian and Paleozoic basement are affected by faults that are inherited from Variscanorogen and reactivated during Atlasic shortening.

8. Conclusion

This work presents the combine use of Landsat OLI and SRTM data with GIS analysis techniques in order to extract and interpret the geological lineaments in Telouet-Tighza area. A specific methodology for lineament extraction followed in this study allow to delineate more lineament structures in targeted area as well as to compare and combine the output resulted from Oli and SRTM DEM images. The OLI sensor data and SRTM DEM images have proved their usefulness for lineament network mapping due to their high spectral and spatial resolution. Furthermore, the extraction of lineament automatically was demonstrated to be an appropriate technique for lineament analysis. The results of this study showed that the automatic extraction of lineaments minimizes the time spent in classical methods of lineament mapping and yield tangible results. To achieve the aim of this study, several image enhancement techniques including PCA transform, band composite and directional Filters were applied on optical Oli image in order to help the identification of pervasive lineaments in

Telouet-Tighza region. Otherwise, shaded relief images were generated from SRTM DEM in view to recognize geological lineaments and evaluate the structural implication of the lineaments resulted from processing of Landsat 8 oli image. The geologic interpretations of products resulted from the processing of PC1 and 6-5-4 images as well as DEM shaded relief data show that different structural lineaments can be better identified. In addition, the results of this study approve the ability of OIF technique to choose the suitable bands and the efficiency of directional filter efficient in detection of lineament. For validation of the newly developed band image results as well as lineaments obtained from PC1 and shaded relief images, comparison with faults previously digitized manually from geological map was carried out.Finally, after removing non geological features, these results were combined to construct a new synthetic lineament map of Telouet-Tighza area. A total of 3242 widespread lineaments, ranging in size from a few meters to 14 km, with an average length of 2, 28 km were generated from the enhanced remote sensing data. The statistical analysis by using rose diagram showed that lineaments extracted are grouped in two families with average orientations ENE-WSW and E-W and dominance of the E-W trend. The density maps highlighted also the complementarity between the Oli satellite image and SRTM data in identifying lineaments in studied area and revealed that areas with high density coincide with the major faults existing in geological map of Telouet-Tighza area. Therefore, the involvement of geomorphological and lithological factors to explain lineament distribution revealed that small-scaled distribution of the lineaments was controlled by a combine effect of lithological and topographical factors whereas their spatial distribution at large scale was generated by several orogenic phases structured High Atlas belt. Our approach of integrating Landsat 8- Oli images and SRTM DEM data with thematic geological map leaded to effective lineament mapping in the Telouet- Tighza area and has delivered encouraging results for using these data. Hence, Landsat digital image processing and enhancement integrated with SRTM radar data are a recommended less time- and cost-consuming approach for detailed lineament mapping in others districts as the Telouet- Tighza shield. It is also advisable to integrate the discriminating band ratio images for control and validation owing to its ability to detect lithological boundaries. The present research might potentially help or guide mineral exploration and groundwater studies in this region.

Abbreviations

SRTM DEM Shuttle Radar Topography Mission Digital Elevation Model

OLI Operational Land Imager

GIS Geographic information system

UTM Universal Transverse Mercator Projection

PCA Principal Component Analysis

PC1 Principal Component 1

BR Bands Ratios

CC Color Composite

DF Directional Filtering

OIF optimum Index Factor

ENVI Environment for Visualizing Images

FLAASH Fast Line-of-sight Atmospheric Analysis of Spectral Hypercubes

Declarations

Acknowledgements

This article is made possible with the assistance and encouragement of both the Faculty of University of Cadi Ayyad. The authors would like to thank the NASA-USGS GLOVIS-GATE for the satellite data (Landsat Oli) and the http://search.asf.alaska.edu for the SRTM radar data. The authors are also very grateful to the anonymous reviewers for their valuable comments and suggestions and to the journal editor for a careful review of the article which helped to present work lucidly.

Compliance with ethical standards

The authors declare that they have no competing interests. The data and material used in thisresearch is partly available in the body of the article; other data/material is also available topublic and will be provided through writing to the corresponding author.

References

1. A., A. Oyawale, O. Adeoti F., R. Ajayi T., and A. Omitogun A. 2020. “Applications of Remote Sensing and Geographic Information System (GIS) in Regional Lineament Mapping and Structural Analysis in Ikare Area, Southwestern Nigeria.” Journal of Geology and Mining Research 12 (1): 13–24. https://doi.org/10.5897/jgmr2019.0310.
2. Abdelkareem, Mohamed, Zakaria Hamimi, Mohammed Z El-Bialy, Hossam Khamis, and Samar A Abdel Wahed. 2021. “Integration of Remote-Sensing Data for Mapping Lithological and Structural Features in the Esh El-Mallaha Area, West Gulf of Suez, Egypt.” Arabian Journal of Geosciences 14 (6): 1–14.
3. Abdelouhed, Farah, Algouti Ahmed, Algouti Abdellah, and Ifkirne Mohammed. 2021. “Lineament Mapping in the Iknioуen Area (Eastern Anti-Atlas, Morocco) Using Landsat-8 Oli and SRTM Data.” Remote Sensing Applications: Society and Environment 23: 100606.
4. Abdelouhed, Farah, Algouti Ahmed, Algouti Abdellah, Ifkirne Mohammed, and Ourhzif Zouhair. 2021. “Extraction and Analysis of Geological Lineaments by Combining ASTER-GDEM and Landsat 8 Image Data in the Central High Atlas of Morocco.” Natural Hazards, 1–23.
5. Abdelouhed, Farah, Ahmed Algouti, Abdellah Algouti, Mohamed Ait Mlouk, and Mohammed Ifkirne. 2021. “Lithological Mapping Using Landsat 8 Oli Multispectral Data in Boumalne, Imider, and Sidi Ali Oubork, High Central Atlas, Morocco.” In E3S Web of Conferences. Vol. 234. EDP Sciences.
6. Adiri, Zakaria, Abderrazak El Harti, Amine Jellouli, Rachid Lhissou, Lhou Maacha, Mohamed Azmi, Mohamed Zouhair, and El Mostafa Bachaoui. 2017. “Comparison of Landsat-8, ASTER and Sentinel 1 Satellite Remote Sensing Data in Automatic Lineaments Extraction: A Case Study of Sidi Flah-Bouskour Inlier, Moroccan Anti Atlas.” Advances in Space Research 60 (11): 2355–67.
7. Adiri, Zakaria, Abderrazak El Harti, Amine Jellouli, Lhou Maacha, and El Mostafa Bachaoui. 2016. “Lithological Mapping Using Landsat 8 OLI and Terra ASTER Multispectral Data in the Bas Drâa Inlier, Moroccan Anti Atlas.” Journal of Applied Remote Sensing 10 (1): 16005.
8. Al-Djazouli, Mahamat Ouchar, Karim Elmorabiti, Basem Zoheir, Abdelmejid Rahimi, and Omayma Amellah. 2019. “Use of Landsat-8 OLI Data for Delineating Fracture Systems in Subsoil Regions: Implications for Groundwater Prospection in the Waddai Area, Eastern Chad.” Arabian Journal of Geosciences 12 (7): 1–15.
9. Aldharab, Hamdi S, Syed Ahmad Ali, Javed Ikbal, and Saleh A Ghareb. 2018. “Spatial Analysis of Lineaments and Their Tectonic Significance Using Landsat Imagery in Alarasah Area-Southeastern Central Yemen.” J Geogr Environ Earth Sci Int 18 (2): 1–13.
10. Algouti, A. 1991. “Turonien Supérieur et Sénonien Du Versant Nord Du Haut-Atlas de Marrakech: Caractérisation Sédimentologique et Stratigraphique.” https://toubkal.imist.ma/handle/123456789/1834.
11. Amer, Reda, Timothy Kusky, and Abduwasit Ghulam. 2010. “Lithological Mapping in the Central Eastern Desert of Egypt Using ASTER Data.” Journal of African Earth Sciences 56 (2–3): 75–82.
12. Arabi, El Hassane El, Jose Bienvenido Diez, Jean Broutin, and Rachid Essamoud. 2006. “First Palynological Characterization of the Middle Triassic; Implications for the First Tethysian Rifting Phase in Morocco.” Comptes Rendus Geoscience 338 (9): 641–49.
13. Aretouyap, Zakari, Lawal Billa, Matthew Jones, and Goetz Richter. 2020. “Geospatial and Statistical Interpretation of Lineaments: Salinity Intrusion in the Kribi-Campo Coastland of Cameroon.” Advances in Space Research 66 (4): 844–53.
14. Arifin, Ainyyafiatty, Nor Aizam Adnan, and Abdul Rauf Abdul Rasam. 2021. “Multi-Sensor Assessment of Geological Lineament Detection.” IOP Conference Series: Earth and Environmental Science 767 (1). https://doi.org/10.1088/1755-1315/767/1/012014.
15. Azman, Ali Imran, Jasmi Ab Talib, and Mohamad Shaufi Sokiman. 2020. “The Integration of Remote Sensing Data for Lineament Mapping in the Semanggol Formation, Northwest Peninsular Malaysia.” In IOP Conference Series: Earth and Environmental Science, 540:12026. IOP Publishing.
16. Bentahar, Ibtissame, Mohammed Raji, and Hicham Si Mhamdi. 2020. “Fracture Network Mapping Using Landsat-8 OLI, Sentinel-2A, ASTER, and ASTER-GDEM Data, in the Rich Area (Central High Atlas, Morocco).” Arabian Journal of Geosciences 13 (16): 1–19.
17. Bentahar, Ibtissame, Mohammed Raji, and Hicham Si Mhamdi. 2020. “Fracture Network Mapping Using Landsat-8 OLI, Sentinel-2A, ASTER, and ASTER-GDEM Data, in the Rich Area (Central High Atlas, Morocco).” Arabian Journal of Geosciences 13 (16). https://doi.org/10.1007/s12517-020-05736-6.
18. Biron, Pierre, and Bernard Courtinat. 1982. “Contribution Palynologique à La Connaissance Du Triasdu Haut-Atlas de Marrakech, Maroc.” Geobios 15 (2): 231–35.
19. Brahim, L Ait, P Chotin, S Hinaj, A Abdelouafi, A El Adraoui, Ch Nakcha, D Dhont, M Charroud, F Sossey Alaoui, and M Amrhar. 2002. “Paleostress Evolution in the Moroccan African Margin from Triassic to Present.” Tectonophysics 357 (1–4): 187–205.
20. Cavallina, C, M Papini, G Moratti, and M Benvenuti. 2018. “The Late Mesozoic Evolution of the Central High Atlas Domain (Morocco): Evidence from the Paleo-Drainage Record of the Adrar Aglagal Syncline.” Sedimentary Geology 376: 1–17.
21. Chavez, P S, BERLIN GL, and SOWERS LB. 1982. “Statistical Method for Selecting Landsat MSS Ratios.”
22. Choubert, Georges, and Willy Chazan. 1957. “Bibliographie Régionale. Maroc (Suite).” Bulletin de Minéralogie 80 (4): 245–50.
23. Choubert, Georges, and Anne Faure-Muret. 1962. Le Séisme d’Agadir, Ses Effets et Son Interprétation Géologique. Service de la carte géologique.
24. Cirés, J, J Marturià, A De Paz, J Casanovas, and A Lleopart. 1997. “Digital Elevation Models, a Useful Tool for Geological Mapping. Some Examples from Catalonia.” In Second Congress on Regional Geological Cartography and Information Systems, 297–304.
25. Courtinat, Bernard, and Abdellah Algouti. 1985. “Caractérisation Probable Du Sinémurien Près de Telouat (Haut-Atlas, Maroc): Datation Palynologique.” Geobios 18 (6): 857–67.

26. Domènech, Mireia, Antonio Teixell, Julien Babault, and Maria-Luisa Arboleya. 2015. “The Inverted Triassic Rift of the Marrakech High Atlas: A Reappraisal of Basin Geometries and Faulting Histories.” Tectonophysics 663: 177–91.
27. Elmahdy, Samy Ismail, Mohamed Mostafa Mohamed, and Tarig A. Ali. 2021. “Automated Detection of Lineaments Express Geological Linear Features of a Tropical Region Using Topographic Fabric Grain Algorithm and the SRTM DEM.” Geocarto International 36 (1): 76–95. https://doi.org/10.1080/10106049.2019.1594393.
28. Epuh, Emeka E, Chukwuma J Okolie, Olagoke E Daramola, Funmilola S Ogunlade, Funmilayo J Oyatayo, Samuel A Akinnusi, and Eno-Obong I Emmanuel. 2020. “An Integrated Lineament Extraction from Satellite Imagery and Gravity Anomaly Maps for Groundwater Exploration in the Gongola Basin.” Remote Sensing Applications: Society and Environment 20: 100346.
29. Es-Sabbar, Brahim, Mourad Essalhi, Abdelhafid Essalhi, and Hicham Si Mhamdi. 2020. “Lithological and Structural Lineament Mapping from Landsat 8 OLI Images in Ras Kammouna Arid Area (Eastern Anti-Atlas, Morocco).” Economic and Environmental Geology 53 (4): 425–40.
30. Farah, Abdelouhed, Ahmed Algouti, Abdellah Algouti, Maryam Errami, and Mohammed Ifkirne. 2021. “Lithological Mapping and Automatic Lineament Extraction Using Aster and Gdem Data in the Imini-Ounilla-Asfalou District, South High Atlas of Marrakech, Morocco.” In E3S Web of Conferences, 240:4002.
31. Farah, Abdelouhed, Ahmed Algouti, Abdellah Algouti, Mohammed Ifkirne, Aboubakr Ezziyani, and Hdoufane Abdelkarim. 2021. “Mapping of Soil Degradation in Semi-Arid Environments in the Ouarzazate Basin in the South of the Central High Atlas, Morocco, Using Sentinel 2 A Data.” Remote Sensing Applications: Society and Environment, 100548.
32. Farahbakhsh, Ehsan, Rohitash Chandra, Hugo K H Olierook, Richard Scalzo, Chris Clark, Steven M Reddy, and R Dietmar Müller. 2020. “Computer Vision-Based Framework for Extracting Tectonic Lineaments from Optical Remote Sensing Data.” International Journal of Remote Sensing 41 (5): 1760–87.
33. Fekkak, A, H Ouanaimi, A Michard, A Soulaimani, E M Ettachfini, I Berrada, H El Arabi, A Lagnaoui, and O Saddiqi. 2018. “Thick-Skinned Tectonics in a Late Cretaceous-Neogene Intracontinental Belt (High Atlas Mountains, Morocco): The Flat-Ramp Fault Control on Basement Shortening and Cover Folding.” Journal of African Earth Sciences 140: 169–88.
34. Githenya, Lincoln K, Patrick C Kariuki, and Aaron K Waswa. 2019. “Application of Remote Sensing in Mapping Hydrothermal Alteration Zones and Geological Structures as Areas of Economic Mineralization in Mwitika-Makongo Area, SE Kenya.” J Env Earth Sci 13 (2): 11–22.
35. Hamdani, Nadia, and Abdennasser Baali. 2019. “Fracture Network Mapping Using Landsat 8 OLI Data and Linkage with the Karst System: A Case Study of the Moroccan Central Middle Atlas.” Remote Sensing in Earth Systems Sciences 2 (1): 1–17.
36. Han, Ling, Zhiheng Liu, Yuming Ning, and Zhongyang Zhao. 2018. “Extraction and Analysis of Geological Lineaments Combining a DEM and Remote Sensing Images from the Northern Baoji Loess Area.” Advances in Space Research 62 (9): 2480–93.
37. Hermi, Sarra Ouerghi, Ranya Fadlalla Abdalla Elsheikh, Maher Aziz, and Samir Bouaziz. 2017. “Structural Interpretation of Lineaments Uses Satellite Images Processing: A Case Study in North-Eastern Tunisia.” Journal of Geographic Information System 9 (04): 440.
38. Ibouh, H, F El Bchari, M Bouabdelli, A Souhel, and N Youbi. 2001. “L’accident Tizal-Azourki Haut Atlas Central Du Maroc: Déformations Synsedimentaires Liasiques En Extension et Conséquences Du Serrage Atlasique.” Estudios Geologicos 57 (1–2): 15–30.
39. Ibrahim, Umikaltuma, and Felix Mutua. 2014. “Lineament Extraction Using Landsat 8 (OLI) in Gedo, Somalia.” International Journal of Science and Research (IJSR) 3 (9): 291–96.
40. Javhar, Aminov, Xi Chen, Anming Bao, Aminov Jamshed, Mamadjanov Yunus, Aminov Jovid, and Tuerhanjiang Latipa. 2019. “Comparison of Multi-Resolution Optical Landsat-8, Sentinel-2 and Radar Sentinel-1 Data for Automatic Lineament Extraction: A Case Study of Alichur Area, SE Pamir.” Remote Sensing 11 (7): 778.
41. Jawahar Raj, N, and A Prabhakaran. 2018. “Lineaments of Kodaikanal-Palani Massif, Southern Granulitic Terrain of Tamil Nadu, India: A Study Using SRTM DEM and LANDSAT Satellite’s OLI Sensor’s FCC.” Geology, Ecology, and Landscapes 2 (3): 188–202.
42. Jellouli, Amine, Abderrazak El Harti, Zakaria Adiri, Mohcine Chakouri, Jaouad El Hachimi, and El Mostafa Bachaoui. 2021. “Application of Optical and Radar Satellite Images for Mapping Tectonic Lineaments in Kerdous Inlier of the Anti-Atlas Belt, Morocco.” Remote Sensing Applications: Society and Environment 22: 100509.
43. Kolawole, M S, J M Ishaku, A Daniel, and O D Owonipa. 2016. “Lineament Mapping and Groundwater Occurrence within the Vicinity of Osara Dam, Itakpe-Okene Area, North Central Nigeria, Using Landsat Data.” Journal of Geosciences and Geomatics 4 (3): 42–52.
44. Leprêtre, R, Y Missenard, J Barbarand, C Gautheron, I Jouvie, and O Saddiqi. 2018. “Polyphased Inversions of an Intracontinental Rift: Case Study of the Marrakech High Atlas, Morocco.” Tectonics 37 (3): 818–41.
45. Masoud, A A, and K Koike. 2006. “Arid Land Salinization Detected by Remotely-Sensed Landcover Changes: A Case Study in the Siwa Region, NW Egypt.” Journal of Arid Environments 66 (1): 151–67.
46. Mhamdi, Hicham Si, Mohammed Raji, Soufiane Maimouni, and Mostafa Oukassou. 2017. “Fractures Network Mapping Using Remote Sensing in the Paleozoic Massif of Tichka (Western High Atlas, Morocco).” Arabian Journal of Geosciences 10 (5): 125.
47. Michard, André, Hassan Ibouh, and André Charrière. 2011. “Syncline-topped Anticlinal Ridges from the High Atlas: A Moroccan Conundrum, and Inspiring Structures from the Syrian Arc, Israel.” Terra Nova 23 (5): 314–23.
48. Missenard, Yves, Zouhair Taki, Dominique Frizon de Lamotte, Mohamed Benammi, Mohamad Hafid, Pascale Leturmy, and Michel Sébrier. 2007. “Tectonic Styles in the Marrakesh High Atlas (Morocco): The Role of Heritage and Mechanical Stratigraphy.” Journal of African Earth Sciences 48 (4): 247–66.
49. Moret, L. n.d. “Carte Géologique de l’Atlas de Marrakech Au 1/200. 000 et Notice Explicative.” 1931 35.
50. Nedjraoui, Khedoudja, Mohamed Hamoudi, Riad Ben El Khaznadji, Samir Oughou, and Abderrahmane Bendaoud. 2021. “Structural Mapping and Interpretation of Lineaments Related to the In Teria Volcanism (Southeastern Algeria) Using Landsat 8 OLI TIRS Images and Aeromagnetic Data.” Journal

of African Earth Sciences 184 (August): 104348. https://doi.org/10.1016/j.jafrearsci.2021.104348.

51. Okeke, C. J., V. U. Ukaegbu, and N. Egesi. 2019. “Remote Sensing Signature of Geological Structures Inferred on Landsat Imagery of Afikpo Area Southeastern Nigeria.” Journal of Geology and Mining Research 11 (1): 1–13. https://doi.org/10.5897/jgmr2018.0305.
52. Ouanaimi, Hassan. 1989. “Evolution Sédimentaire et Tectonique de La Partie Orientale de Massif Ancien Du Haut-Atlas(Maroc).”
53. Pearson, Karl. 1901. “LIII. On Lines and Planes of Closest Fit to Systems of Points in Space.” The London, Edinburgh, and Dublin Philosophical Magazine and Journal of Science 2 (11): 559–72.
54. Perez, Nicholas D., Antonio Teixell, David Gómez-Gras, and Daniel F. Stockli. 2019. “Reconstructing Extensional Basin Architecture and Provenance in the Marrakech High Atlas of Morocco: Implications for Rift Basins and Inversion Tectonics.” Tectonics 38 (5): 1584–1608. https://doi.org/10.1029/2018TC005413.
55. Pour, AB, M Hashim - Journal of Asian Earth Sciences, and undefined 2011. n.d. “Identification of Hydrothermal Alteration Minerals for Exploring of Porphyry Copper Deposit Using ASTER Data, SE Iran.” Elsevier. Accessed January 13, 2021. https://www.sciencedirect.com/science/article/pii/S136791201100294X.
56. Pour, Amin Beiranvand, and Mazlan Hashim. 2015. “Hydrothermal Alteration Mapping from Landsat-8 Data, Sar Cheshmeh Copper Mining District, South-Eastern Islamic Republic of Iran.” Journal of Taibah University for Science 9 (2): 155–66.
57. Pour, Amin Beiranvand, Mazlan Hashim, Charles Makoundi, and Khin Zaw. 2016. “Structural Mapping of the Bentong-Raub Suture Zone Using PALSAR Remote Sensing Data, Peninsular Malaysia: Implications for Sediment-hosted/Orogenic Gold Mineral Systems Exploration.” Resource Geology 66 (4): 368–85.
58. Saadi, Nureddin M, M Abdel Zaher, F El-Baz, and Koichiro Watanabe. 2011. “Integrated Remote Sensing Data Utilization for Investigating Structural and Tectonic History of the Ghadames Basin, Libya.” International Journal of Applied Earth Observation and Geoinformation 13 (5): 778–91.
59. Saddiqi, O, L Baidder, and A Michard. 2011. “Haut Atlas et Anti-Atlas, Circuit Oriental.” Nouveaux Guides Géologiques et Miniers Du Maroc, Edited by A. Michard et Al., Notes Mem. Serv. Geol. Maroc 557: 1–111.
60. Saidi, Omar, Hicham Si Mhamdi, Abdelhafid Essalhi, and Abdeslam Toummite. 2020. “Fracture Network Mapping Using Landsat-8 OLI Images of the Mining Zone of Jbel Tijekht in Moroccan Eastern Anti-Atlas.” Estudios Geológicos 76 (2): e133.
61. Salui, Chalantika Laha. 2018. “Methodological Validation for Automated Lineament Extraction by LINE Method in PCI Geomatica and MATLAB Based Hough Transformation.” Journal of the Geological Society of India 92 (3): 321–28.
62. Sedrette, Slimen, and Noamen Rebai. 2016. “Automatic Extraction of Lineaments from Landsat Etm+ Images and Their Structural Interpretation: Case Study in Nefza Region (North West of Tunisia).” Journal of Research in Environmental and Earth Sciences 4 (2016): 139–45.
63. Shandini, Yves, Marcelin Pemi Mouzong, Raphael Onguene, Minette Eyango Tomedi, Jacques Etame, and Bernard Zobo Essimbi. 2020. “Automatic Extraction and Geospatial Analysis of Lineaments and Their Tectonic Significance in South Cameroon Area Using Remote Sensing Techniques and GIS.” Anuário Do Instituto de Geociências 43 (4): 319–29.
64. Singh, Kamini, Ajay Kumar Arya, and Kamal Kishore Agarwal. 2020. “Landslide Occurrences Along Lineaments on NH-154A, Chamba, Himachal Pradesh; Extracted from Satellite Data Landsat 8, India.” Journal of the Indian Society of Remote Sensing 48 (5): 791–803. https://doi.org/10.1007/s12524-020-01113-8.
65. Thannoun, Rayan Ghazi. 2013. “Automatic Extraction and Geospatial Analysis of Lineaments and Their Tectonic Significance in Some Areas of Northern Iraq Using Remote Sensing Techniques and GIS.” International Journal Of Enhanced Research In Science Technology & Engineering Bulletin 2 (2): 1–11.
66. Xu, Junlong, Xingping Wen, Haonan Zhang, Dayou Luo, Jinbo Li, Lianglong Xu, and Min Yu. 2020. “Automatic Extraction of Lineaments Based on Wavelet Edge Detection and Aided Tracking by Hillshade.” Advances in Space Research 65 (1): 506–17. https://doi.org/10.1016/j.asr.2019.09.045.
67. Ye, Bei, Shufang Tian, Jia Ge, and Yaqin Sun. 2017. “Assessment of WorldView-3 Data for Lithological Mapping.” Remote Sensing 9 (11): 1–19. https://doi.org/10.3390/rs9111132.
68. Yu, Le, Alok Porwal, Eun Jung Holden, and Michael C. Dentith. 2012. “Towards Automatic Lithological Classification from Remote Sensing Data Using Support Vector Machines.” Computers and Geosciences 45: 229–39. https://doi.org/10.1016/j.cageo.2011.11.019.

Figures

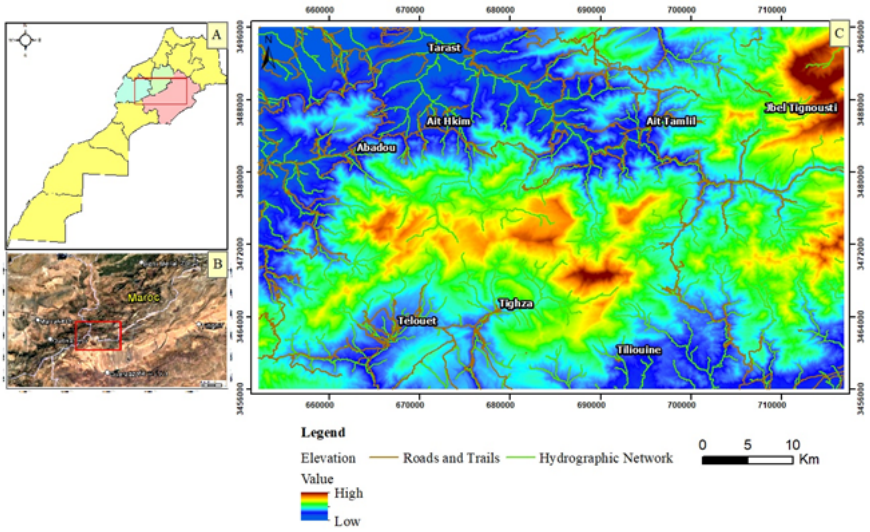

Figure 1

Location of the study area, at Moroccan view (A) and at the Regional and provincial view (B). (C); the elevation model of the studied area.

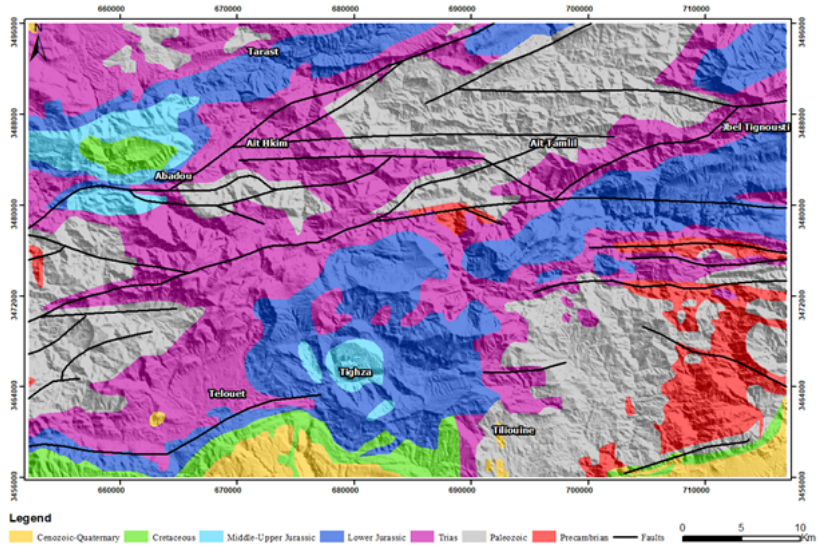

Figure 2

The subset geo-structural map of Telouet-Tighza area extracted from the geological map of Morocco at 1:1000000 scale (Ministry of Energy and Mines, Geology Directorate).

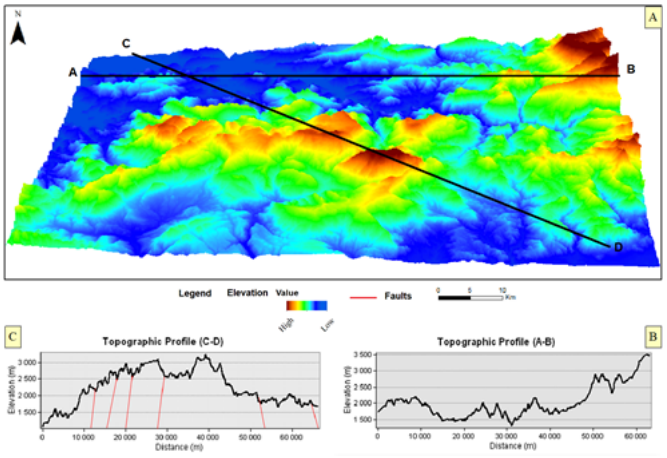

Figure 3

(A); 3D representation of the Digital Elevation Model of the study area with an exaggeration of 2m to the vertical. (B); Topographic profile of the study area along AB section and (C); Topographic profile of the study area along CD section with major faults

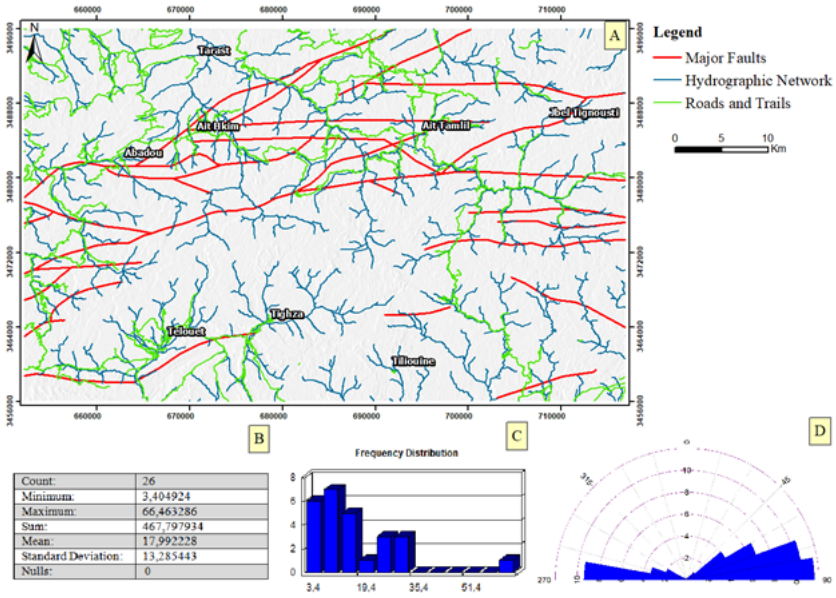

Figure 4

(A) Major faults digitized from the geological map of the study area. (B) Basic statistics of lineaments extracted; (C) Length frequency diagram of lineaments and (D) Rose diagram of lineaments extracted.

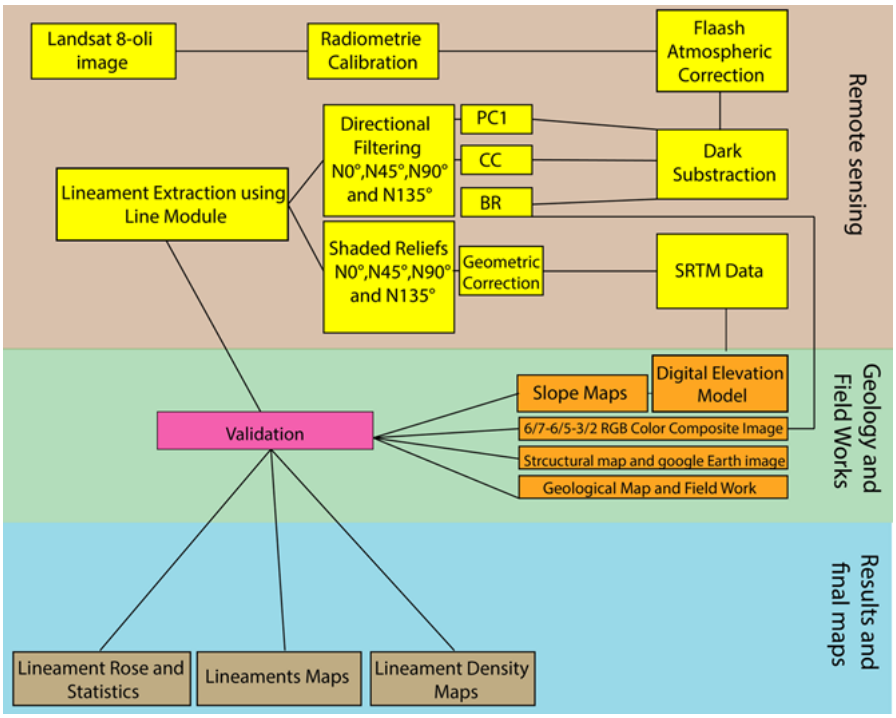

Figure 5

Methodology flowchart of the present study

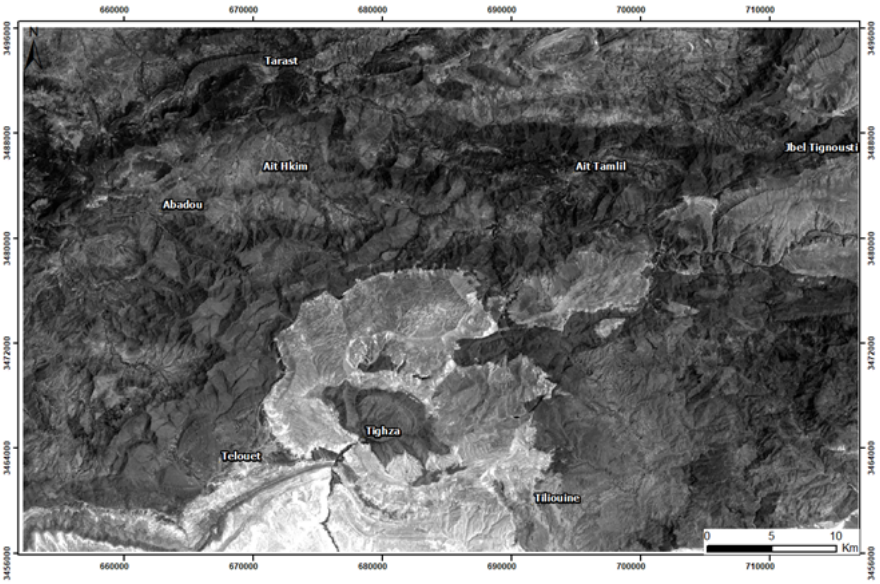

Figure 6

PC1 image derived from OLI data

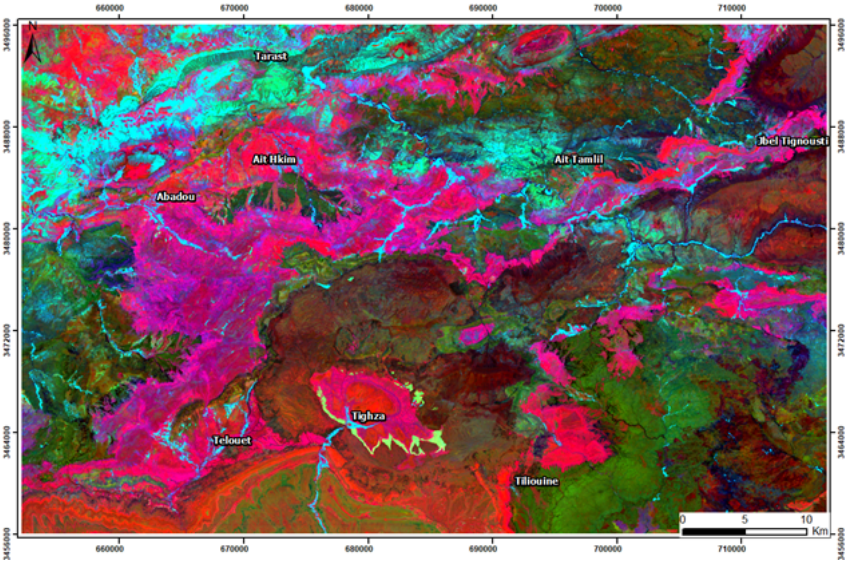

Figure 7

6-5-7 Color Composite Bands image in RGB.

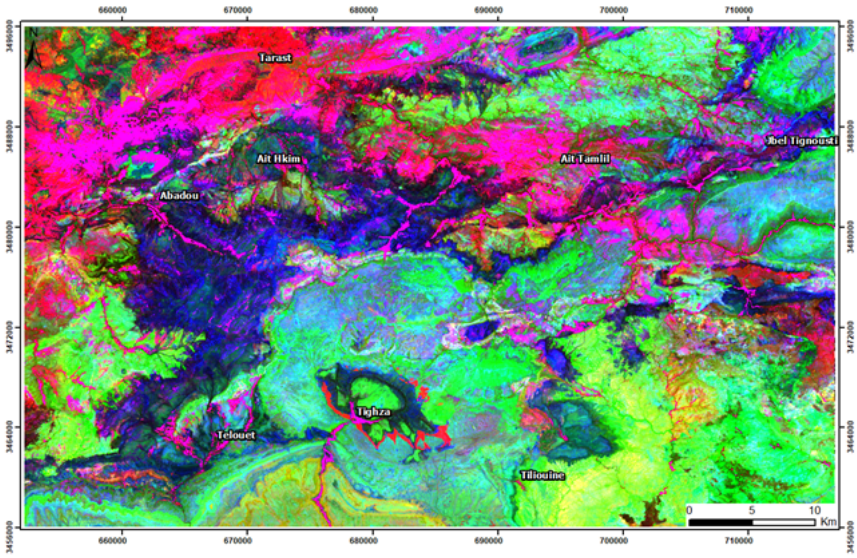

Figure 8

6/7-6/5-3/2band ratio composite image generated from Oli bands.

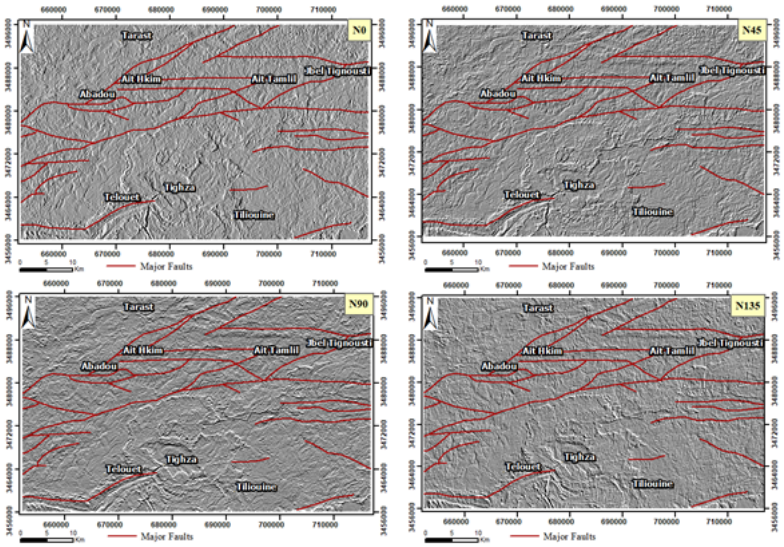

Figure 9

Four subset filtered images generated from PC1 of Landsat-8 OLI image.

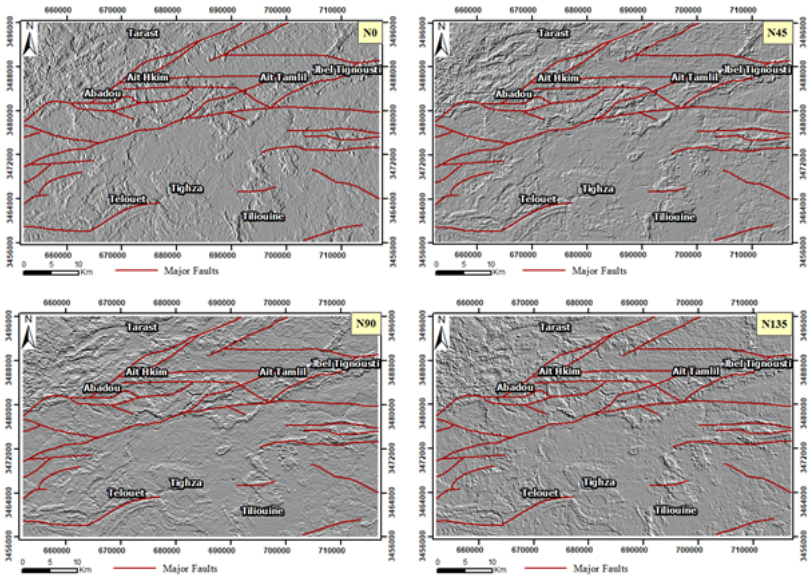

Figure 10

Four subset filtered images derived from 6-5- 7 composite bands image of Landsat-8 OLI.

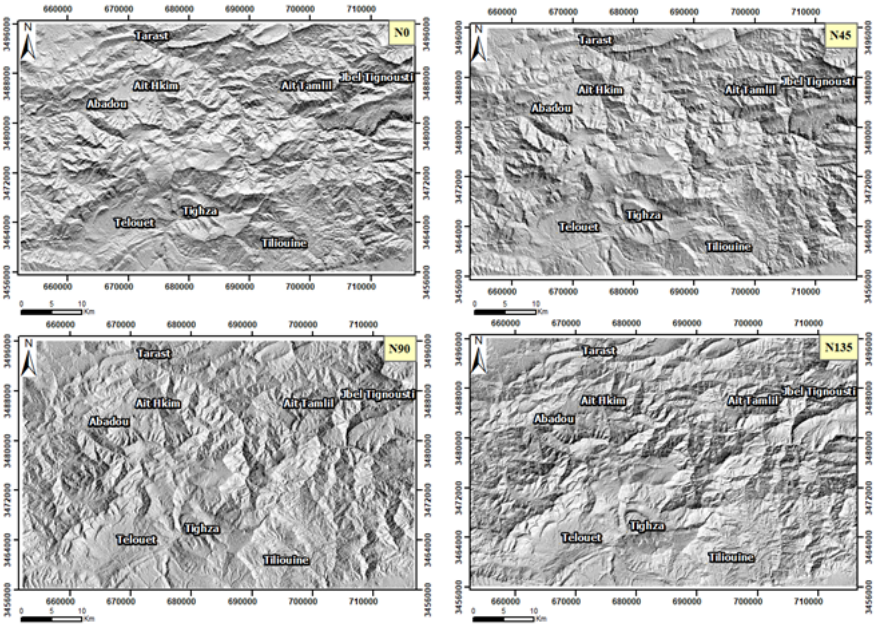

Figure 11

Four shaded relief images generated from SRTM.

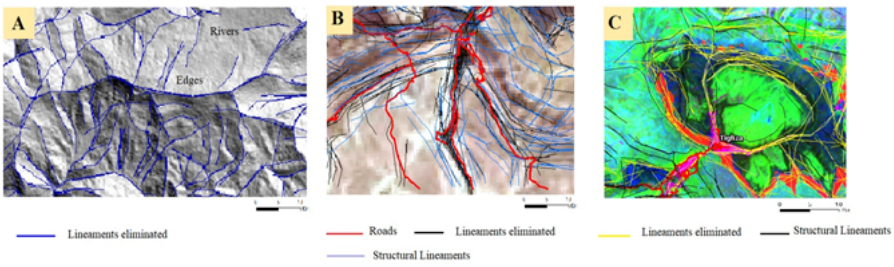

Figure 12

Examples of non-geological lineaments, A Edge lines and Rivers, B Roads, and C lithological boundaries

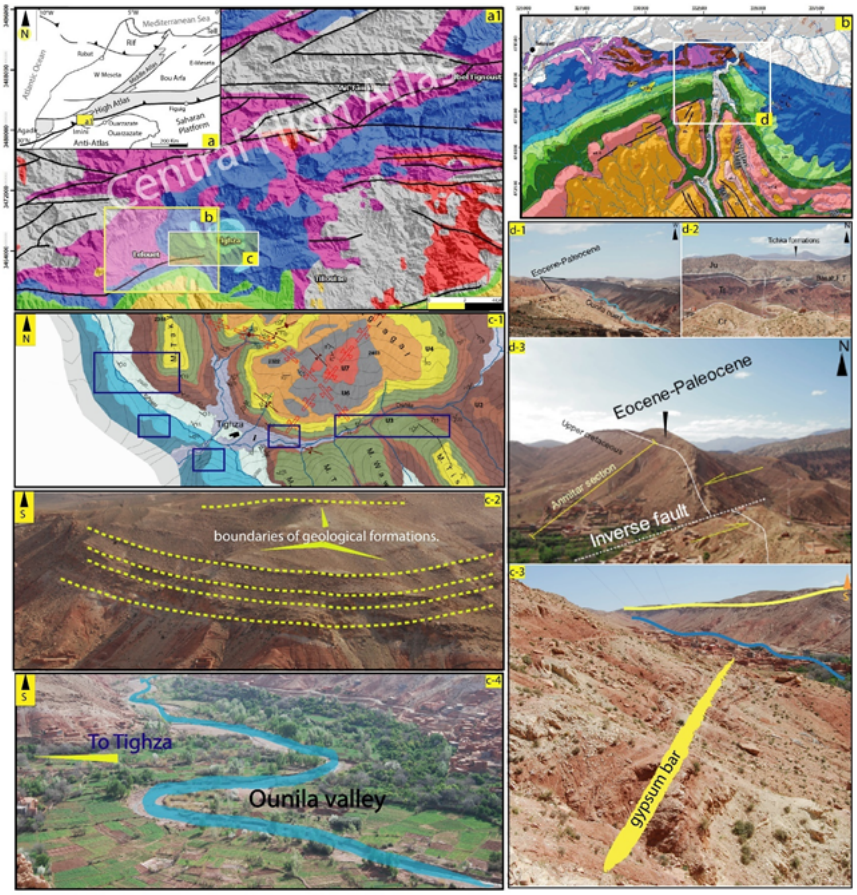

Figure 13

(a) ,location of the study area on the border of the Marrakech High Atlas on a structural map of the Moroccan High Atlas,(a1) The subset geo-structural map of Telouet-Tighza area extracted from the geological map of Morocco at 1:1000000 scale (Ministry of Energy and Mines, Geology Directorate).this map representing the major and various lineaments of the area,(b), local geological framework of the study area showing the different geological outcrops (d1,d2 and d3), different structural and nonstructural lineaments validated in the field work (Tighza Douar),(c1,c2,c3 and c4),some validation of the lineaments and non-lineaments structures at the level of Tighza area as it is located on the map produced by(Cavallina et al. 2018) in c3,(non geological lineaments; Oued, limits of the geological formations).

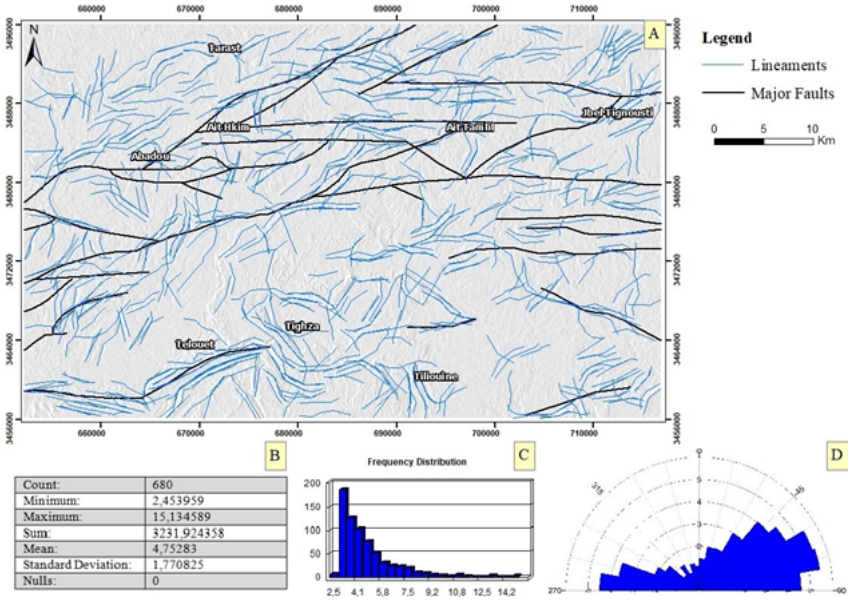

Figure 14

(A) Synthetic lineaments maps derived from PC1 image after elimination of non-geological lineaments. (B) Basic statistics of lineaments extracted (C) Length frequency diagram of lineaments, and (D) Rose diagram of lineaments extracted.

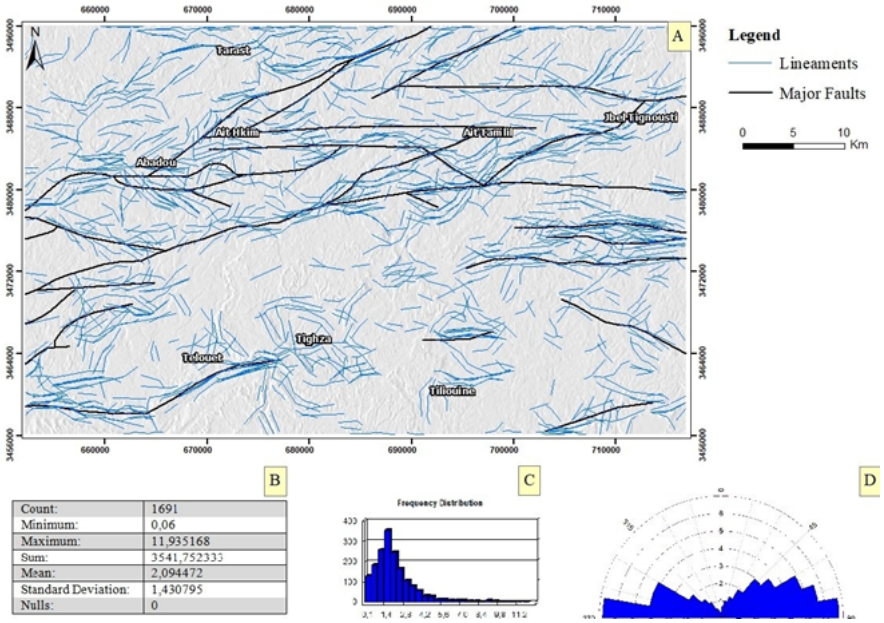

Figure 15

(A) Synthetic lineaments maps from 6-5- 7 RGB image after elimination of non-geological lineaments Basic statistics of lineaments extracted, (B) Basic statistics of lineaments extracted, (C)Length frequency diagram of lineaments, and (D) Rose diagram of lineaments extracted.

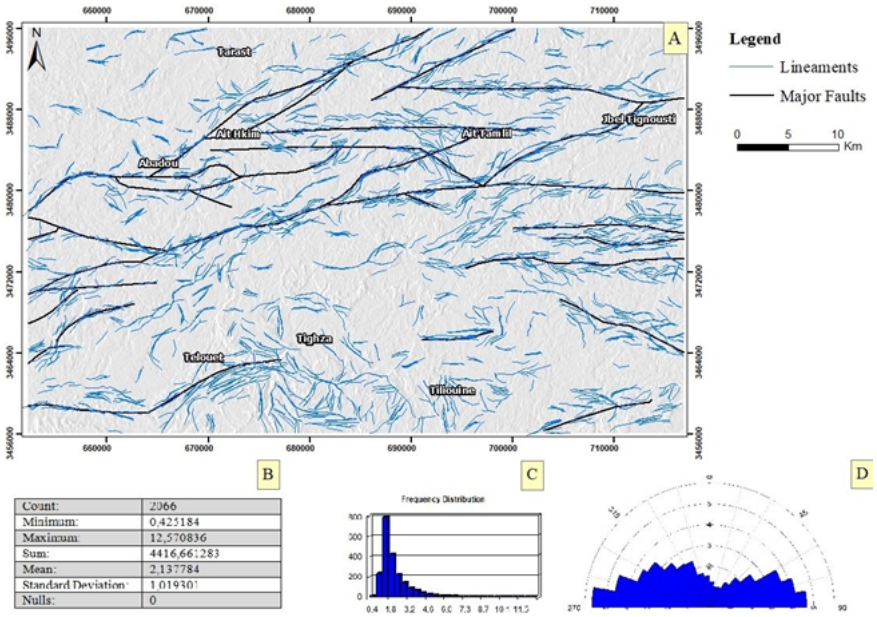

Figure 16

(A) Synthetic lineaments maps from SRTM image (12 m of resolution) after elimination of non-geological lineaments Basic statistics of lineaments extracted, (B) Basic statistics of lineaments extracted, (C)Length frequency diagram of lineaments, and (D) Rose diagram of lineaments.

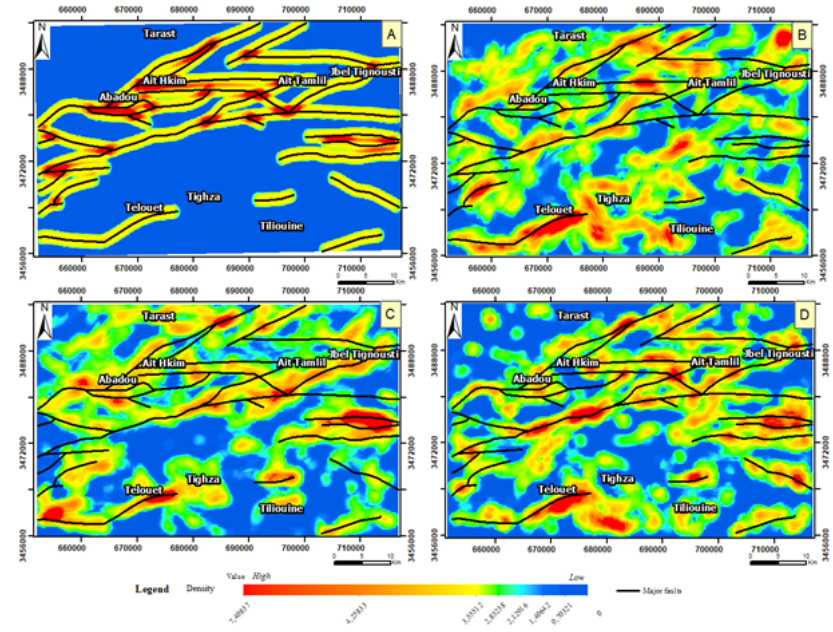

Figure 17

Overlay of Major faults and fractures of Telouet-Tighza area on the lineament densities automatically generated from (A) the geological map, (B) the PC1 image of the Landsat 8 Oli image, (C) the 6-5-7 bands composite image and (D) SRTM image.

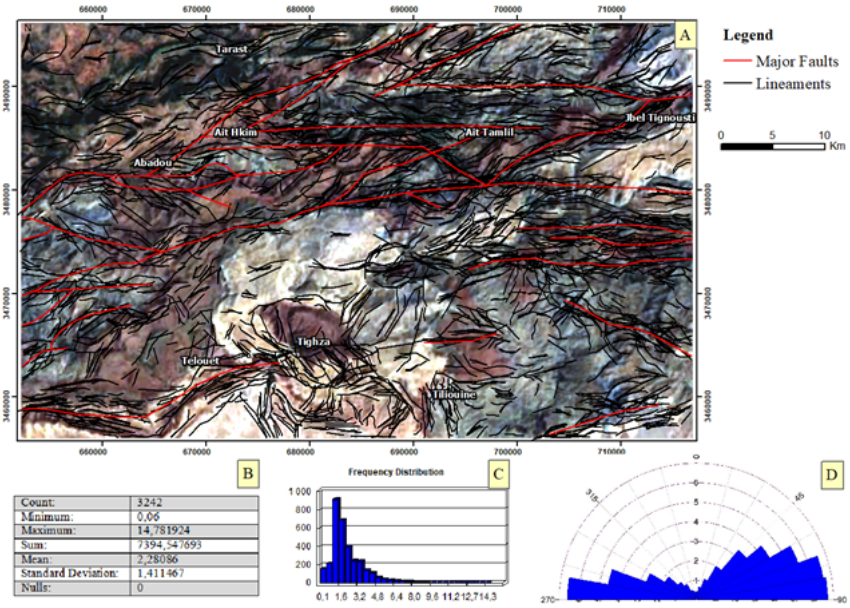

Figure 18

Final map showing the all extracted lineaments and major existing faults superimposed to the high-resolution Google Earth image. ((B) Basic statistics of all lineaments extracted, (C) Length frequency diagram of all lineaments, and (D) Rose diagram of lineaments

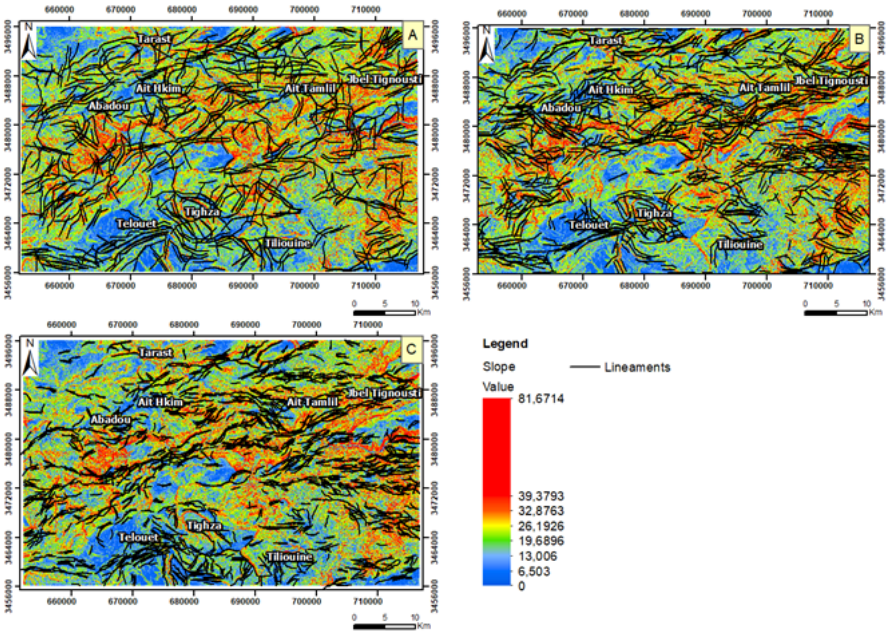

Figure 19

Superposition of slope image and lineaments maps generated from (A) PC1 image, (B) 6-5-7 bands composite image of Landsat- 8 OLI and (C) SRTM image.

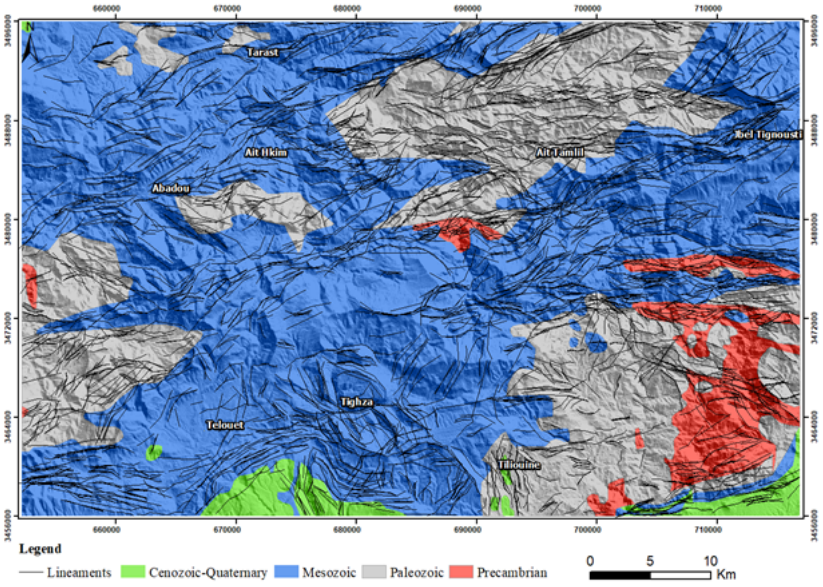

Figure 20

Superposition of all lineaments extracted from Landsat-8 Oli image and SRTM data on the lithological map of the study area (subset from the geological map of Morocco at 1:1000000 scale (Ministry of Energy and Mines, Geology Directorate).